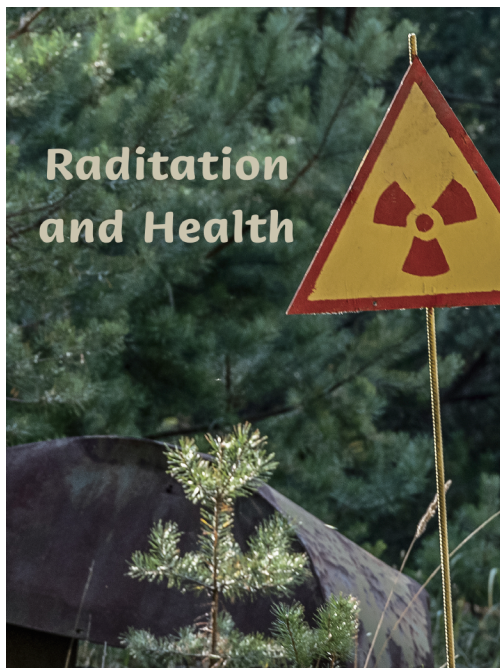


# CHINA CDC WEEKLY



## 中国疾病预防控制中心周报



### Preplanned Studies

National Monitoring and Analysis of Internal Exposure of Nuclear Medicine Workers in <sup>131</sup> I Treatment — China, 2021–2023	353
Two-Year Surveillance of Dengue, Zika, and Chikungunya Viruses Among Chinese Blood Donors — Guangxi and Yunnan PLADs, China, 2022–2023	357
Developing Machine Learning Models Based on Clinical Manifestations to Predict Influenza — Chongqing Municipality, China, 2022–2023	363
Infodemic Management and Public Health Emergency Preparedness Capacities — Khyber Pakhtunkhwa, Pakistan, 2024	368

### Methods and Applications

A Prediction Model and Method for Indoor Radon Concentration by A Radon Simulation Chamber	374
--	-----



ISSN 2096-7071



## Editorial Board

**Editor-in-Chief** Hongbing Shen

**Founding Editor** George F. Gao

**Deputy Editor-in-Chief** Liming Li    Gabriel M Leung    Zijian Feng

**Executive Editor** Chihong Zhao

### Members of the Editorial Board

Rui Chen	Wen Chen	Xi Chen (USA)	Zhuo Chen (USA)
Gangqiang Ding	Xiaoping Dong	Pei Gao	Mengjie Han
Yuantaao Hao	Na He	Yuping He	Guoqing Hu
Zhibin Hu	Yueqin Huang	Na Jia	Weihua Jia
Zhongwei Jia	Guangfu Jin	Xi Jin	Biao Kan
Haidong Kan	Ni Li	Qun Li	Ying Li
Zhenjun Li	Min Liu	Qiyong Liu	Xiangfeng Lu
Jun Lyu	Huilai Ma	Jiaqi Ma	Chen Mao
Xiaoping Miao	Ron Moolenaar (USA)	Daxin Ni	An Pan
Lance Rodewald (USA)	William W. Schluter (USA)	Yiming Shao	Xiaoming Shi
Yuelong Shu	RJ Simonds (USA)	Xuemei Su	Chengye Sun
Quanfu Sun	Xin Sun	Feng Tan	Jinling Tang
Huaqing Wang	Hui Wang	Linhong Wang	Tong Wang
Guizhen Wu	Jing Wu	Xifeng Wu (USA)	Yongning Wu
Min Xia	Ningshao Xia	Yankai Xia	Lin Xiao
Hongyan Yao	Zundong Yin	Dianke Yu	Hongjie Yu
Shicheng Yu	Ben Zhang	Jun Zhang	Liubo Zhang
Wenhua Zhao	Yanlin Zhao	Xiaoying Zheng	Maigeng Zhou
Xiaonong Zhou	Guihua Zhuang		

## Advisory Board

**Director of the Advisory Board** Jiang Lu

**Vice-Director of the Advisory Board** Yu Wang    Jianjun Liu    Jun Yan

### Members of the Advisory Board

Chen Fu	Gauden Galea (Malta)	Dongfeng Gu	Qing Gu
Yan Guo	Ailan Li	Jiafa Liu	Peilong Liu
Yuanli Liu	Kai Lu	Roberta Ness (USA)	Guang Ning
Minghui Ren	Chen Wang	Hua Wang	Kean Wang
Xiaoqi Wang	Zijun Wang	Fan Wu	Xianping Wu
Jingjing Xi	Jianguo Xu	Gonghuan Yang	Tilahun Yilma (USA)
Guang Zeng	Xiaopeng Zeng	Yonghui Zhang	Bin Zou

## Editorial Office

**Directing Editor** Chihong Zhao

**Managing Editors** Yu Chen

**Senior Scientific Editors** Daxin Ni    Ning Wang    Wenwu Yin    Shicheng Yu    Jianzhong Zhang    Qian Zhu

### Scientific Editors

Weihong Chen	Tao Jiang	Xudong Li	Nankun Liu	Liwei Shi	Liuying Tang
Meng Wang	Zhihui Wang	Qi Yang	Qing Yue	Lijie Zhang	Ying Zhang

## Preplanned Studies

# National Monitoring and Analysis of Internal Exposure of Nuclear Medicine Workers in $^{131}\text{I}$ Treatment — China, 2021–2023

Xiaoliang Li<sup>1</sup>; Jianxiang Liu<sup>1</sup>; Fei Tuo<sup>1</sup>; Weihong Chen<sup>2</sup>; Jianfeng Zhang<sup>1</sup>; Shuo Wang<sup>1</sup>; Quanfu Sun<sup>1,†</sup>

## Summary

### What is already known on this topic?

Healthcare workers in  $^{131}\text{I}$  treatment facilities face potential occupational internal exposure through inhalation of volatile radioiodine, in addition to external exposure.

### What is added by this report?

This study presents the first comprehensive national monitoring data on internal exposure among Chinese nuclear medicine (NM) workers. Approximately one-fifth of personnel working at radioiodine treatment sites showed detectable levels of  $^{131}\text{I}$  in their thyroid tissue.

### What are the implications for public health practice?

These findings provide essential baseline data for enhancing radiation protection protocols in NM facilities and optimizing national internal exposure monitoring.

measurements exceeding  $1.0 \times 10^2$  Bq decreased from 12.8% in 2021 to 10.0% in 2023. The detectable rate varied with job categories ( $P=0.001$ ), with the detectable rate of cleaners being the highest.

**Conclusions:** In China,  $^{131}\text{I}$  was detected in the thyroid of about one-fifth of the subjects working at radioiodine treatment sites. Detectable rate exhibited a slow downward trend in recent years.

The average annual external exposure doses for medical radiation workers in China have shown a significant decline from 1.4 mSv (1996–2000) (1) to 0.35 mSv (2016) (2). However, beyond external exposure, nuclear medicine (NM) workers face additional risks from potential internal contamination due to their work with unsealed radiopharmaceuticals (3). Among these radionuclides,  $^{131}\text{I}$  presents the primary internal exposure risk due to its high volatility and extended half-life.

This study aimed to assess internal exposure levels among NM staff across various hospitals to inform the development of evidence-based management and employee protection strategies. Following pilot measurements of  $^{131}\text{I}$  internal exposure in NM workers from 2018 to 2020, the study expanded to include 29 provincial-level administrative divisions (PLADs) from 2021 to 2023 ( $^{131}\text{I}$  monitoring was not conducted in Shanxi in 2023). We present a comprehensive analysis of  $^{131}\text{I}$  treatment practices across China and evaluate thyroid  $^{131}\text{I}$  activity levels among staff at radioiodine treatment facilities during this period. The findings are intended to provide an empirical foundation for enhancing radiation protection protocols for personnel working at radioiodine treatment facilities throughout China.

This study comprised two main components. First, information about NM hospitals was collected through questionnaires, encompassing all non-military hospitals in China with NM programs. Second, portable gamma

## ABSTRACT

**Introduction:** The effective dose caused by the external exposure of medical radiation workers has dramatically declined in China. By contrast, less attention has been given to internal exposure to radiation. This study aimed to describe the national monitoring of the internal exposure of Chinese nuclear medicine (NM) workers from 2021 to 2023. These findings provide essential baseline data for enhancing radiation protection protocols in NM facilities and optimizing national internal exposure monitoring.

**Methods:** All the non-military hospitals in China with an NM program were investigated. Portable gamma spectrometers were used to measure the  $^{131}\text{I}$  activities of the thyroid of staff members at  $^{131}\text{I}$  treatment sites.

**Results:** A total of 998 hospitals in China had an NM program in 2023. Detectable rate (measurements above minimum detectable activity) decreased from 26.2% in 2021 to 20.1% in 2023. The proportion of

spectrometers were calibrated using  $^{131}\text{I}$  standard sources at our institution for thyroid activity measurements. The calibrated equipment was used to measure  $^{131}\text{I}$  activities in the thyroid of selected staff members at  $^{131}\text{I}$  treatment facilities. A standardized measurement and calculation protocol was developed into a handbook and disseminated through training to detection institutions. The detector was consistently positioned in contact with either the neck or thigh (for background measurement), with a measurement duration of 120 s. Minimum detectable activity (MDA) was employed to characterize the gamma spectrometer's capability in quantifying radionuclide presence. The detailed methodology for calculating thyroid  $^{131}\text{I}$  activity and MDA has been previously published (4). All data were uploaded through the National Radiological Health Information Platform and analyzed using Microsoft Excel 2016 (Microsoft Corporation, Redmond, WA., USA) and SPSS software (version 20.0; IBM, Armonk, USA). Statistical significance was defined as a two-sided  $P < 0.05$ .

In 2023, China had 998 hospitals with NM programs, employing 11,285 workers across all PLADs except Xizang Autonomous Region. Of these institutions, 637 (63.8%) hospitals with 8,818 NM workers conducted  $^{131}\text{I}$  treatment procedures, and 358 (35.9%) hospitals with 5,893 workers specifically performed  $^{131}\text{I}$  treatment for thyroid cancer. Surface contamination monitors were available in 906 (90.8%) hospitals. Among the 637 hospitals providing  $^{131}\text{I}$  treatment, 62.6% were equipped with automated  $^{131}\text{I}$  loading devices (Supplementary Table S1, available at <http://weekly.chinacdc.cn/>).

National internal exposure monitoring of staff at radioiodine treatment sites commenced in 2021. Table 1 presents the comprehensive monitoring results from 2021 to 2023. The number of monitored hospitals increased from 255 in 2021 to 405 in 2023, with participating staff members rising from 1,884 to 3,137. Both the detectable rate (measurements above MDA) and the proportion of measurements exceeding

$1.0 \times 10^2$  Bq have showed a consistent decline since 2021.

In 2023, thyroid  $^{131}\text{I}$  activity measurements were conducted on 3,137 staff members from radioiodine treatment sites across 29 PLADs (Supplementary Table S2, available at <http://weekly.chinacdc.cn/>).  $^{131}\text{I}$  was detected in the thyroid of 630 participants (20.1%), with the maximum measurement reaching  $5.8 \times 10^4$  Bq. Further evaluation was performed on measurements exceeding  $1.0 \times 10^2$  Bq, which represented 10.0% of all participants.

Analysis revealed no significant gender-based differences in detectable rates ( $P = 0.443$ ). However, operators exhibited a significantly higher detectable rate (25.7%) compared to nonoperators (18.2%) ( $P < 0.001$ ). Detectable rates varied significantly across job categories ( $P = 0.001$ ). Notably, cleaners, despite not directly operating  $^{131}\text{I}$  equipment, demonstrated the highest detectable rate, followed by nurses. Detailed distributions are presented in Table 2.

Among the 908 participants who had operated  $^{131}\text{I}$  during the previous year, 899 provided data regarding their most recent  $^{131}\text{I}$  operation timing. Analysis of the relationship between measurement timing and detectable rates revealed a clear temporal pattern (Figure 1). The highest detectable rate of 47.4% occurred when measurements were performed on the same day as  $^{131}\text{I}$  operations. This rate decreased significantly to 31.6% after just one day and continued to decline progressively with increasing time intervals ( $P < 0.001$ ).

## DISCUSSION

Our analysis revealed that 998 hospitals in China, employing 11,285 staff members, maintained NM programs in 2023. Approximately two-thirds of these NM facilities provide  $^{131}\text{I}$  treatment services, while one-third specifically conduct  $^{131}\text{I}$  treatment for thyroid cancer. The latter requires substantially higher radioiodine doses compared to hyperthyroidism treatment protocols.

TABLE 1. Measurements of  $^{131}\text{I}$  activities in the thyroid of staff members at radioiodine treatment sites in China, 2021–2023.

Year	PLADs numbers	Hospitals numbers	Participants numbers	Detectable rate (%)	Maximum $^{131}\text{I}$ thyroid activity (Bq)	Proportion of measurements above $1.0 \times 10^2$ Bq (%)
2021	22	255	1,884	26.2	$4.4 \times 10^4$	12.8
2022	20	287	2,210	21.7	$2.9 \times 10^4$	11.3
2023	29	405	3,137	20.1	$5.8 \times 10^4$	10.0

Note: Military hospitals are not included in this study.

Abbreviation: PLADs=provincial-level administrative divisions.

Despite a gradual decline in detectable rates from 2021 to 2023,  $^{131}\text{I}$  was still detected in the thyroids of approximately one-fifth of workers at radioiodine treatment sites. This detectable rate falls between those reported in previous studies, being lower than the approximately 30% observed in Polish research (5) but higher than the 15% reported in Korean investigations (6). These variations may be attributed to differences in  $^{131}\text{I}$  exposure frequency and radiation protection protocols across countries.

The detectable rate exhibits substantial provincial variation, which may be attributed to differences in radiation protection protocols and sample sizes. Provinces with higher detectable rates require enhanced attention to internal contamination monitoring of nuclear medicine workers. Our stratified analysis revealed that nuclear medicine operators had significantly higher detectable rates compared to nonoperators. Furthermore, we identified a negative correlation between the time interval from operation to detection and the detectable rate.

Notably, cleaners exhibited the highest detectable rate among all nuclear medicine workers, despite not directly operating equipment. This elevated risk stems from their prolonged exposure during the cleaning of radioiodine treatment sites, combined with inadequate personal radiation protection (7). The high detectable rate among cleaners likely results primarily from insufficient awareness of self-protection protocols, highlighting the need for enhanced radiation protection training in nuclear medicine facilities. Implementation of basic protective measures, such as wearing charcoal masks and medical rubber gloves, can significantly reduce  $^{131}\text{I}$  intake through inhalation and

ingestion. The relatively uniform detectable rates observed among other worker categories may be attributed to varied patterns of  $^{131}\text{I}$  handling, as all workers except cleaners regularly engage in direct  $^{131}\text{I}$  manipulation.

While our findings suggest that increasing the intervals between  $^{131}\text{I}$  operations could reduce radiation exposure risk, excessive extension of these intervals may prove counterproductive. Prolonged periods between operations could lead to degradation

TABLE 2. Distribution of the participants above MDA in different groups.

Item	Participants numbers	Above MDA		P
		Numbers	Proportion (%)	
Gender				0.443
Male	1,372	267	19.5	
Female	1,765	363	20.6	
$^{131}\text{I}$ operation				<0.001
No	2,186	397	18.2	
Yes	908	233	25.7	
Job				0.001
Cleaners	156	44	28.2	
Nurses	806	190	23.6	
Doctors	1,273	241	18.9	
Others	140	25	17.9	
Technicians	762	130	17.1	

Note: Others include physicists, chemists and pharmaceutical engineers. In 2023, thyroid  $^{131}\text{I}$  activity measurements were conducted on 3,137 staff members, but the information on  $^{131}\text{I}$  operation for 43 subjects is missing.  $^{131}\text{I}$  was detected in the thyroids of 630 participants (20.1%).

Abbreviation: MDA=minimum detectable activity.

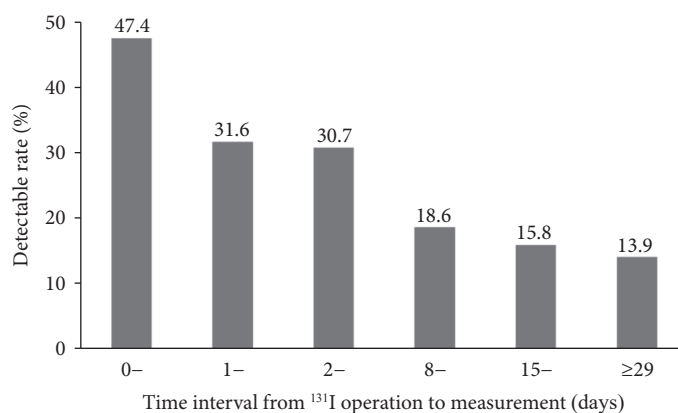


FIGURE 1. Detectable rate of different time intervals from  $^{131}\text{I}$  operation to measurement in 2023.

Note: A total of 899 measurements are shown in this figure, because the time intervals from  $^{131}\text{I}$  operation to measurement for 8 subjects are missing. Linear-by-linear association chi-squared test suggested that the trend of detectable rate exhibited statistical significance ( $P < 0.001$ ).

of technical skills, potentially increasing the risk of radioactive contamination. Therefore, establishing optimal rotation schedules for  $^{131}\text{I}$  operations should be a key consideration in daily operational protocols.

This study had a notable limitation regarding the variability in MDA and measurement uncertainty across different monitoring institutions due to the use of diverse portable gamma spectrometers. To enable meaningful comparisons of measurements across PLADs, we standardized the analysis by calculating the proportion of measurements exceeding  $1.0 \times 10^2$  Bq, as all MDAs were below this threshold. Future monitoring efforts should prioritize the standardization of gamma spectrometry equipment. Additionally, occupational radiation dose assessment should incorporate both external exposure and committed doses from radionuclide intake during the same period (8). However, committed doses from internal exposure were not estimated as measurements were conducted only once per year. This limitation arises from the restricted availability of internal exposure monitoring capabilities, with only approximately 70 qualified institutions nationwide. Switzerland's approach of using screening measurements performed by local staff with their own instrumentation offers an economical and practical alternative (9). In future work, we aim to develop a scientific and economic routine monitoring program to accurately assess the committed effective doses of NM workers.

The national screening program conducted over the past three years has yielded valuable data on thyroid  $^{131}\text{I}$  levels among NM workers and their provincial distribution patterns. Through detailed analysis, we identified key factors contributing to elevated detectable rates. These findings provide an essential scientific foundation for enhancing radiation protection protocols in NM facilities and optimizing national internal exposure monitoring systems.

**Conflict of interest:** The authors declare no conflicts of interest.

**Acknowledgments:** The authors gratefully acknowledge the support provided by the Core Competence Training Program of Epidemiology and Health Statistics, Chinese Center for Disease Control and Prevention.

**Ethical statements:** Received ethics approval from the Institutional Ethics Committee of the National

Institute for Radiological Protection, Chinese Center for Disease Control and Prevention (No.LLSC2020-006).

doi: 10.46234/ccdcw2025.057

# Corresponding author: Quanfu Sun, sunquanfu@nirp.chinacdc.cn.

<sup>1</sup> Key Laboratory of Radiological Protection and Nuclear Emergency, National Institute for Radiological Protection, Chinese Center for Disease Control and Prevention, Beijing, China; <sup>2</sup> Department of Occupational and Environmental Health, School of Public Health, Tongji Medical College, Huazhong University of Science and Technology, Wuhan City, Hubei Province, China.

Copyright © 2025 by Chinese Center for Disease Control and Prevention. All content is distributed under a Creative Commons Attribution Non Commercial License 4.0 (CC BY-NC).

Submitted: September 07, 2024

Accepted: February 05, 2025

Issued: March 14, 2025

## REFERENCES

1. Wu WZ, Zhang WY, Cheng RL, Zhang LA. Occupational exposures of Chinese medical radiation workers in 1986-2000. *Radiat Prot Dosimetry* 2005;117(4):440 – 3. <https://doi.org/10.1093/rpd/nci312>.
2. Deng J, Fan SN, Wang T, Hao SX, Liu XH, Guo W, et al. Trends and distribution analysis of occupational exposure from medical practices in China (2010-2016). *Health Phys* 2019;117(6):656 – 60. <https://doi.org/10.1097/HP.0000000000001118>.
3. Wang HB, Zhang QZ, Zhang Z, Hou CS, Li WL, Yang H, et al. Necessity of internal monitoring for nuclear medicine staff in a large specialized Chinese hospital. *Int J Environ Res Public Health* 2016;13(4):418. <https://doi.org/10.3390/ijerph13040418>.
4. Li XL, Zhang JF, Wang S, Liu JX, Tuo F, Sun QF. Measurements of  $^{131}\text{I}$  activity in thyroid of workers at the place of radioiodine therapy in 38 hospitals in China. *J Radiat Res* 2024;65(4):459 – 66. <https://doi.org/10.1093/jrr/rrae036>.
5. Krajewska G, Krajewski P. Evaluation of internal exposure of nuclear medicine staff working with radioiodine in Poland. *Int J Occup Med Environ Health* 2023;36(5):587 – 95. <https://doi.org/10.13075/ijomeh.1896.02136>.
6. Kim ST, Yoo JR, Park JM. An investigation into internal exposure management needs for nuclear medicine practitioners and temporary visitors through I-131 internal dose assessment: focusing on large hospitals in South Korea. *PLoS One* 2018;13(12):e0209244. <https://doi.org/10.1371/journal.pone.0209244>.
7. Guo Y, Zhang XZ, Li DM, Zhang SY, Hu JF, Cheng XJ. Occupational health management of dispatched cleaning personnel at the nuclear medicine workplace in a medical institution. *Chin J Radiol Med Prot* 2021;41(6):461 – 4. <https://doi.org/10.3760/cma.j.issn.0254-5098.2021.06.011>.
8. International Atomic Energy Agency. Radiation protection and safety of radiation sources: international basic safety standards. Vienna: IAEA; 2014.
9. Baechler S, Stritt N, Bochud FO. Individual monitoring of internal exposure for nuclear medicine workers in Switzerland. *Radiat Prot Dosimetry* 2011;144(1-4):464 – 7. <https://doi.org/10.1093/rpd/ncq350>.

## SUPPLEMENTARY MATERIAL

SUPPLEMENTARY TABLE S1. Overview of <sup>131</sup>I treatment and distribution of relevant equipment for nuclear medicine hospitals in China, 2023.

PLADs	NM hospital numbers	NM worker numbers	Tertiary NM hospitals numbers (%)	Performing <sup>131</sup> I treatment		Performing <sup>131</sup> I treatment for thyroid cancer		Equipment numbers of automatic loading devices (%)	Equipment numbers of surface contamination monitors (%)
				Hospitals numbers (%)	Worker numbers (%)	Hospitals numbers (%)	Worker numbers (%)		
Beijing	41	596	34 (82.9)	25 (61.0)	394 (66.1)	4 (9.8)	56 (9.4)	12.0	100
Tianjin	17	243	17 (100)	8 (47.1)	168 (69.1)	4 (23.5)	122 (50.2)	50.0	100
Hebei	45	423	34 (75.6)	29 (64.4)	335 (79.2)	18 (40.0)	239 (56.5)	48.3	100
Shanxi	27	295	23 (85.2)	21 (77.8)	234 (79.3)	15 (55.6)	182 (61.7)	81.0	100
Inner Mongolia	18	169	16 (88.9)	13 (72.2)	137 (81.1)	8 (44.4)	108 (63.9)	46.2	83.3
Liaoning	35	384	32 (91.4)	13 (37.1)	255 (66.4)	12 (34.3)	226 (58.9)	76.9	97.1
Jilin	17	239	17 (100)	11 (64.7)	196 (82.0)	9 (52.9)	177 (74.1)	81.8	94.1
Heilongjiang	20	249	20 (100)	15 (75.0)	226 (90.8)	11 (55.0)	188 (75.5)	73.3	95.0
Shanghai	49	618	32 (65.3)	24 (49.0)	385 (62.3)	8 (16.3)	225 (36.4)	20.8	95.9
Jiangsu	76	801	60 (78.9)	41 (53.9)	501 (62.5)	22 (28.9)	300 (37.5)	43.9	15.8
Zhejiang	41	542	32 (78.0)	23 (56.1)	415 (76.6)	14 (34.1)	268 (49.4)	87.0	92.7
Anhui	38	343	34 (89.5)	24 (63.2)	273 (79.6)	17 (44.7)	213 (62.1)	66.7	100
Fujian	39	355	34 (87.2)	23 (59.0)	285 (80.3)	13 (33.3)	216 (60.8)	34.8	94.9
Jiangxi	33	275	25 (75.8)	21 (63.6)	213 (77.5)	7 (21.2)	100 (36.4)	76.2	93.9
Shandong	60	657	56 (93.3)	38 (63.3)	528 (80.4)	31 (51.7)	447 (68.0)	89.5	100
Henan	55	690	47 (85.5)	37 (67.3)	585 (84.8)	25 (45.5)	479 (69.4)	78.4	100
Hubei	44	592	39 (88.6)	30 (68.2)	485 (81.9)	22 (50.0)	431 (72.8)	83.3	100
Hunan	47	425	38 (80.9)	31 (66.0)	338 (79.5)	10 (21.3)	131 (30.8)	71.0	100
Guangdong	75	969	67 (89.3)	58 (77.3)	871 (89.9)	27 (36.0)	459 (47.4)	48.3	94.7
Guangxi	56	522	48 (85.7)	45 (80.4)	441 (84.5)	15 (26.8)	221 (42.3)	66.7	98.2
Hainan	8	106	7 (87.5)	8 (100)	106 (100)	6 (75.0)	97 (91.5)	87.5	100
Chongqing	34	313	21 (61.8)	17 (50.0)	249 (79.6)	7 (20.6)	133 (42.5)	82.4	97.1
Sichuan	54	571	45 (83.3)	35 (64.8)	471 (82.5)	20 (37.0)	346 (60.6)	65.7	90.7
Guizhou	10	123	10 (100)	8 (80.0)	114 (92.7)	7 (70.0)	106 (86.2)	100	100
Yunnan	20	293	17 (85.0)	14 (70.0)	242 (82.6)	8 (40.0)	157 (53.6)	71.4	95.0
Shaanxi	18	252	15 (83.3)	8 (44.4)	153 (60.7)	3 (16.7)	79 (31.3)	37.5	100
Gansu	9	95	8 (88.9)	7 (77.8)	84 (88.4)	6 (66.7)	73 (76.8)	28.6	100
Qinghai	3	26	3 (100)	2 (66.7)	21 (80.8)	2 (66.7)	21 (80.8)	50.0	66.7
Ningxia	2	34	2 (100)	2 (100)	34 (100)	2 (100)	34 (100)	100	100
Xinjiang	7	85	6 (85.7)	6 (85.7)	79 (92.9)	5 (71.4)	59 (69.4)	66.7	100

Note: Military hospitals were not included in this investigation. In 2023, China had 998 hospitals with nuclear medicine (NM) programs, employing 11,285 workers across all PLADs except Xizang Autonomous Region. Of these institutions, 637 (63.8%) hospitals with 8,818 (78.1%) NM workers conducted <sup>131</sup>I treatment procedures, and 358 (35.9%) hospitals with 5,893 (52.2%) workers specifically performed <sup>131</sup>I treatment for thyroid cancer. Surface contamination monitors were available in 906 (90.8%) hospitals. Among the 637 hospitals providing <sup>131</sup>I treatment, 62.6% were equipped with automated <sup>131</sup>I loading devices.

Abbreviation: PLADs=provincial-level administrative divisions; NM=nuclear medicine.

SUPPLEMENTARY TABLE S2. Distribution of  $^{131}\text{I}$  thyroid activity measurements among staff at radioiodine treatment facilities in China, 2023.

PLADs	Participant numbers	Above MDA		Maximum $^{131}\text{I}$ activities (Bq)	$^{131}\text{I}$ activities above $1.0 \times 10^2$ Bq	
		Numbers	Proportion (%)		Numbers	Proportion (%)
Beijing	106	7	6.6	$3.2 \times 10^3$	7	6.6
Tianjin	19	14	73.7	$2.0 \times 10^3$	1	5.3
Hebei	30	14	46.7	$8.2 \times 10^2$	12	40.0
Inner Mongolia	5	4	80.0	$9.0 \times 10^2$	3	60.0
Liaoning	86	13	15.1	$1.0 \times 10^3$	7	8.1
Jilin	102	14	13.7	$2.2 \times 10^2$	7	6.9
Heilongjiang	200	4	2.0	$5.5 \times 10^2$	4	2.0
Shanghai	204	6	2.9	$5.8 \times 10^4$	3	1.5
Jiangsu	200	46	23.0	$1.0 \times 10^2$	0	0
Zhejiang	96	49	51.0	$6.3 \times 10^2$	8	8.3
Anhui	213	72	33.8	$1.8 \times 10^4$	40	18.8
Fujian	231	58	25.1	$2.2 \times 10^3$	45	19.5
Jiangxi	103	22	21.4	$1.5 \times 10^4$	21	20.4
Shandong	49	43	87.8	$3.1 \times 10^3$	21	42.9
Henan	276	61	22.1	$4.3 \times 10^3$	40	14.5
Hubei	172	27	15.7	$1.2 \times 10^3$	18	10.5
Hunan	44	1	2.3	$1.1 \times 10^2$	1	2.3
Guangdong	276	23	8.3	$1.8 \times 10^2$	6	2.2
Guangxi	252	33	13.1	$3.6 \times 10^3$	14	5.6
Hainan	57	2	3.5	40	0	0
Chongqing	120	27	22.5	$2.7 \times 10^3$	16	13.3
Sichuan	59	9	15.3	$1.1 \times 10^3$	7	11.9
Guizhou	49	12	24.5	$5.4 \times 10^2$	12	24.5
Yunnan	33	9	27.3	$1.0 \times 10^3$	6	18.2
Shaanxi	7	7	100	$5.2 \times 10^2$	5	71.4
Gansu	56	37	66.1	$1.2 \times 10^3$	3	5.4
Qinghai	22	0	0	-	0	0
Ningxia	18	3	16.7	$4.0 \times 10^2$	3	16.7
Xinjiang	52	13	25.0	$1.8 \times 10^3$	4	7.7

Note: No  $^{131}\text{I}$  treatment facilities were present in Xizang in 2023, and  $^{131}\text{I}$  monitoring was not conducted in Shanxi province in 2023. Military hospitals were excluded from this study. In 2023, thyroid  $^{131}\text{I}$  activity measurements were conducted on 3,137 staff members from radioiodine treatment sites.  $^{131}\text{I}$  was detected in the thyroid of 630 participants (20.1%), with the maximum measurement reaching  $5.8 \times 10^4$  Bq. Further evaluation was performed on measurements exceeding  $1.0 \times 10^2$  Bq, which represented 10.0% of all participants.

“-” indicates that the maximum  $^{131}\text{I}$  activity value is not applicable to Qinghai province.

Abbreviation: PLADs=provincial-level administrative divisions; MDA=minimum detectable activity.

## Preplanned Studies

## Two-Year Surveillance of Dengue, Zika, and Chikungunya Viruses Among Chinese Blood Donors — Guangxi and Yunnan PLADs, China, 2022–2023

Ying Yan<sup>1,8</sup>; Xinru Liu<sup>2,8</sup>; Shaofang Lu<sup>3,8</sup>; Le Chang<sup>1,2</sup>; Jing Dong<sup>3</sup>; Huimin Ji<sup>1</sup>; Huizhen Sun<sup>1</sup>; Lunan Wang<sup>1,2,#</sup>

### Summary

#### What is already known about this topic?

The transmission of emerging and re-emerging arboviruses represent a critical challenge to blood transfusion safety worldwide.

#### What is added by this report?

This study established a comprehensive quality assurance system for Dengue virus (DENV), Zika virus (ZIKV), and Chikungunya virus (CHIKV) nucleic acid testing (NAT) blood screening. The system included external quality assessment (EQA) implementation across all participating central blood stations and performance evaluation of six domestic blood screening reagents. Surveillance conducted in Yunnan Province and Guangxi Zhuang Autonomous Region revealed no positive cases among 45,383 blood samples screened in 2022. In 2023, screening of 44,972 blood donors identified 9 NAT-reactive samples at the Xishuangbanna central blood station, with 6 confirmed as DENV-1 positive.

#### What are the implications for public health practice?

Blood stations in border regions must implement comprehensive surveillance systems with enhanced detection sensitivity and robust early warning mechanisms to effectively address emerging disease threats and ensure transfusion safety.

## ABSTRACT

**Introduction:** Emerging and re-emerging transfusion-transmitted arboviruses remain a persistent public health challenge to global blood safety. This study aims to establish a comprehensive nucleic acid testing (NAT) quality control system for Dengue virus (DENV), Zika virus (ZIKV), and Chikungunya virus (CHIKV) screening in blood donations to evaluate the performance of domestic screening reagents, and to assess the prevalence of these arboviruses in border

regions.

**Methods:** Pseudovirus quality control materials based on the Moloney murine leukemia virus (MMLV) vector was constructed to evaluate the limit of detection (LoD) and precision of six blood screening reagents. An external quality assessment (EQA) was conducted across eight central blood stations in Guangxi Zhuang Autonomous Region and Yunnan Provinces. These blood stations employed either reagent A or E for DENV/ZIKV/CHIKV triplex-assay screening of blood donor samples collected during epidemic seasons (June–August) in 2022 and 2023.

**Results:** The six reagents exhibited varied LoD. All evaluated reagents exhibited excellent precision with coefficient of variation (CV) values <5%. All eight central blood stations achieved EQA scores above 80. In 2022, a total of 45,383 blood samples were screened, with no positive cases detected. In 2023, 44,972 blood donors were screened, and nine samples tested positive at the Xishuangbanna central blood station. Confirmatory testing verified six Dengue virus serotype 1 (DENV-1) infections among these cases.

**Conclusions:** This study successfully established a robust quality assurance system for NAT-based arbovirus screening in China. The detection of DENV-positive samples underscore the persisting risk of transfusion-transmitted infections in endemic regions. Continued surveillance and enhanced screening strategies are essential to safeguard blood safety, particularly in arboviral hotspot regions with tropical/subtropical climates prone to recurrent outbreaks.

Emerging and re-emerging transfusion-transmitted diseases represent a critical global threat to blood safety. In China, localized Chikungunya fever outbreaks occurred in Guangdong (2010), Zhejiang (2017), and Yunnan (2019) Provincial-level

administrative division (PLAD), with each occurrence demonstrating progressively longer durations and increasing proportion of imported cases (1). Since 2016, sporadic imported Zika cases have been documented. Between 2010 and 2021, Dengue fever exhibited a biennial outbreak pattern in Yunnan Province, characterized by frequent imported cases and a significant increase in local transmission (2). Given that over 75% of Dengue virus (DENV) infections are asymptomatic, potentially infected blood donors during epidemic periods pose a substantial risk to transfusion safety (3).

RNA detection serves as the earliest marker of acute infection, making nucleic acid testing (NAT) the primary diagnostic tool for accurate arbovirus identification (4). Arbovirus blood screening has been implemented in several countries, with the Asia Pacific Blood Network (APBN) recommending targeted testing in regions experiencing regular seasonal outbreaks (5). Since 2022, the National Health Commission of the People's Republic of China (NHC) has implemented NAT screening for Dengue, Zika, and Chikungunya viruses at eight central blood stations in Yunnan and Guangxi PLAD. This initiative aims to adopt screening strategies based on epidemic trends and enhance blood station screening capabilities, enabling rapid epidemic response. To ensure screening quality, the National Center for Clinical Laboratories (NCCL) has developed quality control materials, evaluated all domestic blood screening reagents, conducting external quality assessments (EQA) for participating blood stations, and provided confirmation testing for screening-reactive samples.

Quality control materials were prepared using Moloney Murine Leukemia Virus (MMLV)-based pseudoviruses containing amplified regions corresponding to all domestic NAT screening reagents used in China. For reagent performance evaluation and EQA, pseudoviruses were quantified via digital PCR and diluted to predetermined concentrations in negative plasma. The limit of detection (LoD) and precision evaluations were conducted in accordance with CLSI EP17-A2, EP15-A3, and CNAS-GL039 guidelines. Annual EQA was performed at eight border central blood stations. (Supplementary Materials, available at <https://weekly.chinacdc.cn/>).

Blood screening for DENV, Zika virus (ZIKV), and Chikungunya virus (CHIKV) was conducted at 8 border central blood stations across 11 cities in Guangxi and Yunnan provinces from June to August

in both 2022 and 2023, using NAT reagents from either Manufacturer A or Manufacturer E. Reactive samples were transported to NCCL for confirmatory testing using five NAT reagents (A, B, C, D, and E), with positive confirmation requiring detection by at least two reagents. Verified positive samples underwent DENV (serotype 1–4) determination using two Real-Time RT-PCR reagents (Shanghai Biogerm Medical Technology Co., LTD, Shanghai, China; Daan Gene Co., LTD, Guangzhou, China) (Figure 1A). Genotype analysis was performed using the NCBI database, and a phylogenetic tree was constructed using the neighbor-joining method in Mega (version 7.0; Mega Development Team). All screened reactive samples underwent serological testing for IgG/IgM (Wondfo Biotech Co., LTD, Guangzhou, China) and Non-structural protein 1 (NS1) antigen (Beijing Wantai Biological Pharmacy Enterprise Co., LTD, Beijing, China).

To ensure screening accuracy, this study validated the limit of detection (LoD) and precision of domestic blood screening reagents. Among the 6 DENV/ZIKV/CHIKV NAT reagents evaluated, reagent C demonstrated superior analytical sensitivity in individual donor NAT (ID-NAT) testing, achieving the lowest LoDs of 12.05 copies/mL for DENV, 13.41 copies/mL for ZIKV, and 14.86 copies/mL for CHIKV. In mini-pool NAT (MP-NAT) testing, reagent C maintained optimal sensitivity for CHIKV (33.24 copies/mL) and DENV (103.94 copies/mL), while reagent A exhibited the lowest LoD for ZIKV at 60.94 copies/mL (Table 1). All kits demonstrated excellent precision, with within-run and within-laboratory coefficient of variation (CV) values below 5% at concentrations of 2 LoD and above (Table 2). The 8 participating blood stations consistently achieved EQA scores exceeding 80 over the 2-year period.

In 2022, the screening of 45,383 blood samples yielded no reactive samples. In 2023, among 44,972 samples screened, 9 DENV-reactive samples (designated 2301–2309) were identified at the Xishuangbanna central blood station using reagent A. Six of these samples were subsequently confirmed as DENV-positive (Figure 1B). Further serotype differentiation revealed all six samples were positive for DENV type 1 (Figure 1C).

All nine reactive samples tested negative for DENV IgG/IgM antibodies. Two samples (2308 and 2309) showed positivity for NS1 antigen. Follow-up testing of sample 2308 at three months post-initial screening

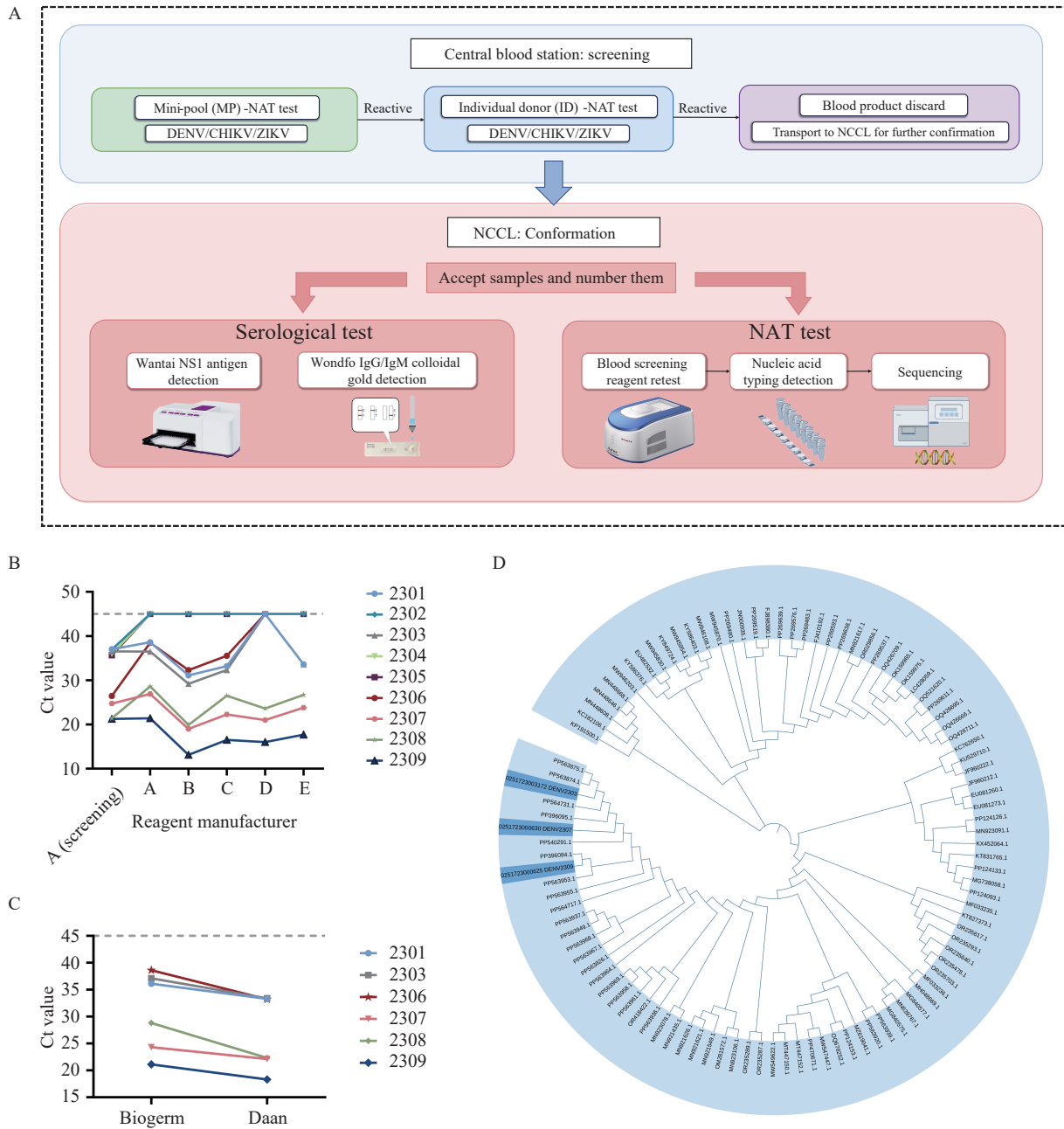


FIGURE 1. Screening and confirmation testing for Dengue, Chikungunya, and Zika viruses. (A) Strategy for screening and confirmation. (B) Results of individual donor testing in screening and retesting of reactive samples using blood screening reagents. (C) Results of DENV serotype differentiation. (D) Phylogenetic tree of E gene of DENV-1 genotype I in Xishuangbanna blood donors.

Note: Samples 2301, 2303, 2306, 2307, 2308, and 2309 demonstrated reactivity in two or more reagents upon retesting and were confirmed as DENV-positive. In panel C, all six samples tested positive for DENV type 1 using DENV typing reagents. Abbreviation: CHIKV=Chikungunya virus; DENV=Dengue virus; ZIKV=Zika virus; NCCL=national center for clinical laboratories; NS1=non-structural protein 1; NAT=nucleic acid testing.

revealed seroconversion with positive DENV IgG/IgM results, while both NS1 antigen and NAT testing were negative, providing definitive evidence of prior DENV infection.

Successful sequencing of samples 2303, 2307, and

2309 identified them as DENV 1 genotype I (Asian type). These strains showed close phylogenetic relationships with contemporary local epidemic strains PP563874/Guangzhou/2023, PP396094/Yunnan/2023, and MW549622/Hainan/2023. Furthermore,

TABLE 1. Limit of detection of six domestic NAT kits for research.

Virus	Test types (copies/mL)	Reagent manufacturer					
		A	B	C	D	E	F
CHIKV	MP-NAT (95% CI)	426.02 (247.86, 978.56)	3,490.82 (2,119.48, 7,909.66)	33.24 (24.72, 72.53)	1,598.18 (1,049.40, 4,868.64)	103.02 (72.04, 195.57)	498.15 (287.16, 1,332.18)
	ID-NAT (95% CI)	36.03 (24.31, 67.31)	428.05 (279.21, 833.91)	14.86 (11.30, 24.79)	375.00	20.04 (13.73, 57.71)	97.14 (57.30, 274.93)
DENV	MP-NAT (95% CI)	605.53 (388.85, 1,163.10)	702.56 (438.75, 1,695.06)	103.94 (72.99, 195.01)	9,809.46 (7,722.29, 16,303.33)	8,178.76 (4,552.37, 19,956.30)	9,209.55 (5,930.77, 19,098.41)
	ID-NAT (95% CI)	199.46 (122.48, 432.15)	218.79 (122.89, 575.78)	12.05 (9.49, 19.21)	8,421.45	907.22 (566.85, 1,867.53)	5,252.56 (3,473.96, 10,411.01)
ZIKV	MP-NAT (95% CI)	60.94 (39.11, 140.65)	379.65 (248.93, 772.45)	168.29 (111.68, 339.06)	2,105.09 (1,433.55, 4,772.67)	129.83 (88.89, 238.80)	217.74 (141.18, 491.16)
	ID-NAT (95% CI)	16.66 (10.15, 44.01)	34.85 (23.70, 77.47)	13.41 (10.32, 22.06)	2,655.70 (1,002.01, 1,881,589.12)	22.70 (15.03, 69.14)	51.51 (36.07, 99.15)

Note: The limit of detection, at which measurement results yielded a positive classification with a 95% probability, was calculated using a probit regression model and is shown with a 95% confidence interval.

Abbreviation: CHIKV=Chikungunya virus; DENV=Dengue virus; ZIKV=Zika virus; NAT=nucleic acid testing; MP-NAT=mini-pool NAT; ID-NAT=individual donor NAT; CI=confidence interval.

TABLE 2. Precision of six domestic NAT kits for research.

Reagent Manufacturer	Precision	MP-NAT									ID-NAT								
		CHIKV			DENV			ZIKV			CHIKV			DENV			ZIKV		
		12,000	1,500	187.5	12,000	1,500	187.5	12,000	1,500	187.5	12,000	1,500	187.5	12,000	1,500	187.5	12,000	1,500	187.5
A	Average Ct value	32.70	35.78		34.14	37.36		28.61	31.67	34.72	30.78	33.53	37.11	31.60	34.69		26.68	29.66	32.83
	Within-run CV (%)	2.22	1.70		0.76	2.01		0.94	1.23	1.30	2.80	2.49	2.38	1.07	1.19		1.76	1.35	1.29
	Within-lab CV (%)	3.81	3.96		1.60	2.44		3.08	2.68	2.67	2.99	5.70	3.52	2.14	1.97		2.50	3.10	1.95
B	Average Ct value	27.90			28.03	31.74		26.34	29.34		25.31	28.87		25.33	28.85		23.65	26.86	
	Within-run CV (%)	1.25			1.01	2.70		1.35	1.20		0.78	1.54		0.79	1.22		0.98	0.92	
	Within-lab CV (%)	2.38			1.41	2.74		1.40	1.50		0.98	2.82		1.31	2.05		1.47	1.70	
C	Average Ct value	32.06	34.94	38.67	33.42	36.98		33.50	36.64		29.45	32.53	35.27	31.05	33.74	37.55	30.64	33.31	36.48
	Within-run CV (%)	1.45	1.02	1.18	1.73	1.83		1.58	1.34		1.45	1.21	0.84	1.78	1.40	1.12	1.72	1.38	1.70
	Within-lab CV (%)	1.73	1.55	1.62	2.94	2.96		1.97	1.69		2.30	1.83	1.69	1.81	1.75	1.63	2.22	2.84	2.40
D	Average Ct value	26.89			30.15			29.59			24.18	27.31		27.54			27.43		
	Within-run CV (%)	0.92			2.14			1.84			0.85	2.13		2.24			1.73		
	Within-lab CV (%)	1.19			2.10			3.47			0.92	2.29		2.71			2.02		
E	Average Ct value	28.47	31.41		33.16			27.63	30.69		26.18	29.35	32.18	31.34	34.31		25.37	28.58	31.43
	Within-run CV (%)	0.40	0.74		0.91			0.37	0.80		0.27	0.32	0.94	0.90	1.11		0.25	0.43	1.14
	Within-lab CV (%)	0.65	0.81		1.36			0.53	0.91		0.53	0.47	0.97	0.93	1.11		0.49	0.62	1.17
F	Average Ct value	31.37	34.25		37.38			32.03	34.46		29.49	32.49		35.79			30.13	32.96	
	Within-run CV (%)	0.84	1.71		3.50			0.83	1.27		0.76	1.11		2.12			1.49	0.84	
	Within-lab CV (%)	2.95	3.03		3.59			2.31	2.27		1.18	1.80		3.89			2.14	2.15	

Abbreviation: CHIKV=Chikungunya virus; DENV=Dengue virus; ZIKV=Zika virus; NAT=nucleic acid testing; MP-NAT=mini-pool NAT; ID-NAT=individual donor NAT; CV=coefficient of variation.

they clustered with viral strains from Singapore (MF033236/Singapore/2015), Malaysia (MH048669/Malaysia/2014), and Thailand (MZ619041/Thailand/2019) (Figure 1D), suggesting importation from Southeast Asian countries.

## DISCUSSION

Blood products play a vital role in healthcare delivery and significantly reduce clinical mortality. However, clinical evidence demonstrates that arboviruses can occasionally cause adverse events through transfusion-transmitted infections (6–7).

This study worked to establish a comprehensive quality assurance system for arbovirus screening by implementing EQA programs for blood stations and evaluating screening reagent performance. All blood stations successfully passed the EQA requirements. The six evaluated kits demonstrated excellent within-run and within-laboratory precision, with CV values below 5%, indicating robust repeatability and reproducibility. However, LoD values varied significantly among reagents and deviated from manufacturer-declared specifications. This variation likely stems from manufacturers using different in-house quality control samples and non-standardized evaluation methods, which were inadequately detailed in their instructions. Our study employed standardized quantitative quality control samples and a unified evaluation protocol, ensuring direct comparability across manufacturers. Notably, domestic blood screening reagents still demonstrate lower sensitivity compared to CE-approved alternatives, such as the Procleix ArboPlex Assay (LoD<17.5 copies/mL), cobas<sup>®</sup>CHIKV/DENV (LoD<7.1 IU/mL) and Cobas<sup>®</sup> Zika (LoD<8.1 copies/mL). Given that the evaluated reagents are currently limited to research use only, manufacturers must significantly enhance product performance before commercial authorization.

DENV, currently the most concerning arbovirus, is transmitted by *Aedes albopictus* and *Aedes aegypti*. Asymptomatic but viremic blood donors pose a significant transfusion safety risk. A systematic review and meta-analysis revealed that NAT screening detected an overall DENV viremic rate of 0.2% among blood donors, with RNA positivity in Southeast Asia at 0.16% (8). This study's screening identified a lower prevalence rate of 1.33‰ (6/44,972) among Chinese blood donors in 2023 compared to Southeast Asian rates. As of April 30, 2024, the World Health

Organization (WHO) has reported over 7.6 million Dengue fever cases worldwide, including 3.4 million confirmed cases, more than 16,000 severe cases, and over 3,000 fatalities across 90 countries with active transmission (9). These findings underscore the necessity for continued arbovirus screening in China's tropical and subtropical regions. However, given China's vast geographical expanse and the regional and seasonal variations in DENV epidemiology, pre-donation health questionnaires may be more cost-effective than universal testing in low-prevalence areas.

In conclusion, this study has successfully established a robust quality control system for NAT screening of DENV/ZIKV/CHIKV in Chinese blood donors. The detection of positive samples in 2023 and the subsequent Dengue outbreak in 2024 emphasize the urgent need to implement comprehensive surveillance and early warning mechanisms, while maintaining readiness in diagnostic capabilities to address emerging health threats.

**Conflicts of interest:** No conflicts of interest.

**Acknowledgements:** The staff members at the central blood stations of Nujiangzhou, Baoshan, Lincang, Wenshanzhou, Honghezhou, Pu'er, Xishuangbanna, and Baise for their contributions to the screening program.

**Ethics statement:** Blood donor screening was conducted in accordance with the "14th Five-Year Plan Work Scheme for Blood Station Blood Safety Monitoring and Risk Early Warning" issued by the National Health Commission. Confirmation testing of reactive samples were approved by the Ethics Committee of Beijing Hospital (2023BJYYEC-443-02).

**Funding:** Supported by the CAMS Innovation Fund for Medical Sciences (CIFMS) (2021-I2M-1-060).

doi: 10.46234/ccdcw2025.058

# Corresponding author: Lunan Wang, lnwang@nccl.org.cn.

<sup>1</sup> National Center for Clinical Laboratories, Institute of Geriatric Medicine, Chinese Academy of Medical Sciences, Beijing Hospital/National Center of Gerontology, Beijing, China; <sup>2</sup> National Center for Clinical Laboratories, Chinese Academy of Medical Sciences & Peking Union Medical College, Beijing, China; <sup>3</sup> Xishuangbanna Central Blood Station, Xishuangbanna City, Yunnan Province, China. <sup>§</sup> Joint first authors.

Copyright © 2025 by Chinese Center for Disease Control and Prevention. All content is distributed under a Creative Commons Attribution Non Commercial License 4.0 (CC BY-NC).

Submitted: August 07, 2024

Accepted: February 08, 2025

Issued: March 14, 2025

## REFERENCES

1. Liu LB, Li M, Gao N, Shen JY, Sheng ZY, Fan DY, et al. Epidemiological and clinical characteristics of the chikungunya outbreak in Ruili City, Yunnan Province, China. *J Med Virol* 2022;94(2):499 – 506. <https://doi.org/10.1002/jmv.27302>.
2. Zhu XX, Wang SW, Li YF, Cao Y, Su XM, Zhao XT. Epidemiological characterization of dengue fever — Yunnan province, China, 2010-2021. *China CDC Wkly* 2024;6(20):457 – 62. <https://doi.org/10.46234/ccdcw2024.088>.
3. Li L, Li Y, Lu SF, Dong J, Xu HX, Zhang Q, et al. Epidemiological survey and screening strategy for dengue virus in blood donors from Yunnan Province. *BMC Infect Dis* 2021;21(1):104. <https://doi.org/10.1186/s12879-021-05810-8>.
4. Munoz-Jordan JL. Diagnosis of Zika virus infections: challenges and opportunities. *J Infect Dis* 2017;216(suppl\_10):S951 – 6. <https://doi.org/10.1093/infdis/jix502>.
5. Asia Pacific Blood Network (APBN). Dengue and the blood supply. White paper updated January 2019. [https://asiapacificbloodnetwork.org/wp-content/uploads/2023/03/apbn\\_white\\_paper\\_dengue\\_v2019\\_final.pdf](https://asiapacificbloodnetwork.org/wp-content/uploads/2023/03/apbn_white_paper_dengue_v2019_final.pdf). [2024-7-29].
6. Guzman MG, Harris E. Dengue. *Lancet* 2015;385(9966):453 – 65. [https://doi.org/10.1016/S0140-6736\(14\)60572-9](https://doi.org/10.1016/S0140-6736(14)60572-9).
7. Viennet E, Frentiu FD, Williams CR, Mincham G, Jansen CC, Montgomery BL, et al. Estimation of mosquito-borne and sexual transmission of Zika virus in Australia: risks to blood transfusion safety. *PLoS Negl Trop Dis* 2020;14(7):e0008438. <https://doi.org/10.1371/journal.pntd.0008438>.
8. Giménez-Richarte Á, Ortiz de Salazar M, Arbona C, Giménez-Richarte MP, Collado M, Fernández PL, et al. Prevalence of Chikungunya, Dengue and Zika viruses in blood donors: a systematic literature review and meta-analysis. *Blood Transfus* 2022;20(4):267 – 80. <https://doi.org/10.2450/2021.0106-21>.
9. World Health Organization. Global arbovirus initiative: preparing for the next pandemic by tackling mosquito-borne viruses with epidemic and pandemic potential. World Health Organization. <https://www.who.int/publications/i/item/9789240088948>. [2024-5-13].

## SUPPLEMENTARY MATERIAL

### Quality Control Materials

The quality control materials were generated using Moloney Murine Leukemia virus (MMLV)-based pseudoviruses. The process involved two key steps: First, the target regions of Dengue virus (DENV), Zika virus (ZIKV), and Chikungunya virus (CHIKV) genomes — specifically those amplified by all domestic DENV/ZIKV/CHIKV triplex nucleic acid testing (NAT) screening reagents in China — were synthesized and inserted into the MMLV vector backbone PQCXIG(w497-1). Second, the resulting plasmids were packaged with pUMVC and pVSVG in 293T cells. The viral supernatant was harvested 48 hours post-transfection and quantified via digital PCR. For reagent performance evaluation and external quality (EQA), the pseudoviruses were diluted to predetermined concentrations in negative plasma. To evaluate reagent performance, pseudoviruses underwent serial two-fold dilutions from 12,000 copies/mL, generating 12 distinct concentrations.

### Limit of Detection

The limit of detection (LoD) evaluation followed the Clinical Laboratory Standards Institute EP17-A2 guideline (Evaluation of Detection Capability for Clinical Laboratory Measurement Procedures; Approved Guideline-Second Edition). Each quality control sample underwent extraction and testing in octuplicate daily for 3 consecutive days. The positive rate for each dilution was calculated, and the LoD was determined using a probit regression model as the measurand concentration yielding positive results with 95% probability. Result interpretation adhered to manufacturer specifications.

### Precision

Precision assessment followed the Clinical Laboratory Standards Institute EP15-A3 guideline (User Verification of Precision and Estimation of Bias; Approved Guideline). Samples at concentrations of 2 LoD and above were tested in quintuplicate daily for 5 consecutive days. Within-run precision (repeatability) and within-laboratory precision were calculated according to guideline specifications.

### External Quality Assessments

National Center for Clinical Laboratories prepared a ten-sample panel comprising negative plasma and positive pseudovirus samples. The EQA utilized a 100-point scoring system, with each sample worth 10 points. Blood stations were required to achieve a minimum score of 80 points based on their qualitative results to pass the assessment.

### Screening of Blood Samples

Blood screening protocols required equipment-compatible reagents from either Manufacturer A or Manufacturer E. Screening was conducted using Multiplex NAT, processing either six samples (Manufacturer A) or eight samples (Manufacturer E) per pool. Individual donor NAT (ID-NAT) was performed on samples from reactive pools to identify specific reactive specimens.

### Genotype Determination

E gene amplification utilized the following primer pairs: F1: 5'-CACATGCCATAGGAACATCCA-3', R1: 5'-ATGAGCCTGTGCACATCACA-3'; F2: 5'-GGAACAGACAAGATTTGCTGGT-3', R2: 5'-TGCCACTTC CACATTTGAGT-3'. The PCR thermal cycling conditions were: 50 °C for 30 min; 94 °C for 2 min; 35 cycles of 94 °C for 30 s, 56 °C for 30 s, 72 °C for 60 s; followed by 72 °C for 7 min, with final hold at 4 °C. Genotype analysis was performed using the NCBI database.

## Preplanned Studies

## Developing Machine Learning Models Based on Clinical Manifestations to Predict Influenza — Chongqing Municipality, China, 2022–2023

Qianqian Zeng<sup>1,8</sup>; Hongyu Zhou<sup>2,8</sup>; Jiang Long<sup>3</sup>; Yi Jian<sup>4</sup>; Li Feng<sup>5</sup>; Liangbo Hu<sup>6</sup>; Hongyu Zhou<sup>6</sup>; Weimin Zhu<sup>1</sup>; Zhe Yuan<sup>1</sup>; Yajuan Chen<sup>1</sup>; Guangzhao Yi<sup>1,9</sup>

### Summary

#### What is already known about this topic?

Current evidence regarding which clinical manifestations best predict influenza requires refinement, particularly considering regional variations in disease presentation and their importance for early diagnosis and surveillance.

#### What is added by this report?

The optimal machine learning model identified key influenza predictors, including epidemiological characteristics, critical symptoms and signs, and age. Based on this model, we introduced a new influenza-like illness (ILI) definition characterized by fever ( $\geq 37.9$  °C) with either cough or rhinorrhea.

#### What are the implications for public health practice?

These findings provide evidence-based clinical manifestations for influenza prediction and offer an optimized definition of ILI for improved surveillance and early detection.

4,249 (36.2%) were confirmed influenza. The predictors of the optimal model included epidemiological characteristics, important symptoms and signs, and age for the total population [Area under curve (AUC) 0.734 (0.710–0.750), accuracy 0.689 (0.669–0.772)]. The new ILI definition was fever ( $\geq 37.9$  °C) with cough or rhinorrhea, and its AUC, sensitivity, and specificity for diagnosing influenza were 0.618 (0.598–0.639), 0.665 and 0.572, outperformed the WHO, China CDC, and USA CDC definitions ( $P < 0.05$ ).

**Conclusions:** Fever, cough, and rhinorrhea maybe the most important indicators for influenza surveillance.

Influenza poses a significant public health threat. Early identification of influenza based on clinical manifestations is crucial for optimal treatment outcomes and prognosis (1). Influenza surveillance serves as a critical component for outbreak early warning systems and timely implementation of preventive and control measures (2). The World Health Organization (WHO) established a global symptom surveillance network for influenza in 1952, known as influenza-like illness (ILI) surveillance (3). However, limited research has evaluated the performance of ILI definition in influenza surveillance using large-scale data from Chinese populations. To address this gap, a retrospective cohort study was conducted at three tertiary comprehensive and influenza sentinel hospitals in Chongqing Municipality, China, between June 2022 and May 2023 (Supplementary Material, available at <https://weekly.chinacdc.cn/>). Our findings demonstrate that body temperature, cough, and rhinorrhea may be the most important clinical indicators for influenza diagnosis and ILI surveillance.

## ABSTRACT

**Introduction:** Clinical manifestations are essential for early diagnosis of influenza-like illness (ILI). Machine learning models for influenza prediction were developed and a new ILI definition was introduced.

**Methods:** A retrospective cohort study was conducted at three hospitals in southwest China during June 2022 and May 2023. Artificial intelligence was used to extract variables from medical records and XGBOOST algorithm was used to develop prediction models for the total population and three age subgroups. A new ILI definition was introduced based on the optimal model and its performance was compared with WHO, China CDC, and USA CDC definitions.

**Results:** Totally 200,135 patients were included.

The study cohort comprised all patients who visited the emergency departments or fever clinics of the three participating hospitals during the study period. Exclusion criteria included: 1) patients who returned to either department for respiratory illness within one month, and 2) patients lacking diagnosis, chief complaint, or present illness history documentation. Laboratory confirmation of influenza infection followed established diagnostic criteria (4). A total of 27 symptom and sign variables were extracted (Supplementary Table S1, available at <https://weekly.chinacdc.cn/>) from the electronic medical record (EMR) information systems of the outpatient and emergency departments. CongRong (Supplementary Material), an artificial intelligence (AI) assistant and pre-trained large language model, was utilized to extract symptom variables for database construction.

The model development and validation dataset comprised cases with confirmed influenza laboratory

testing results. Important variables were identified using the boruta algorithm, and machine learning models were developed for three age subgroups (0–14 years, 15–64 years, and  $\geq 65$  years) and the total population using eXtreme Gradient Boosting (XGBOOST) algorithm (5). For each age group, four models based on different combinations of epidemiological and other variables were constructed, following the process outlined in Supplementary Figure S1 (available at <https://weekly.chinacdc.cn/>). The resulting 16 candidate models were evaluated using the testing dataset (Table 1). The model with the highest area under curve (AUC) of the receiver operating characteristic (ROC) curve was designated as optimal. To interpret the machine learning models, SHapley Additive exPlanations (SHAP) values were employed to quantify the direction and magnitude (mean SHAP value) of important variables in the optimal model (5).

TABLE 1. Performance of machine learning-based prediction models for influenza in the testing dataset.

Dataset	Models	Accuracy (95% CI)	AUC (95% CI)	Threshold <sup>†</sup>	Sensitivity	Specificity
Total population						
	Model_1	0.689 (0.669, 0.772)	0.734 (0.710, 0.750)	0.500	0.541	0.769
	Model_2	0.685 (0.666, 0.703)	0.728 (0.707, 0.749)	0.486	0.525	0.771
	Model_3	0.679 (0.660, 0.698)	0.723 (0.703, 0.744)	0.496	0.535	0.758
	Model_4	0.651 (0.638, 0.670)	0.664 (0.642, 0.687)*	0.483	0.460	0.754
0–14 years age group						
	Model_1	0.607 (0.550, 0.662)	0.680 (0.621, 0.740)	0.500	0.708	0.543
	Model_2	0.604 (0.547, 0.659)	0.680 (0.621, 0.739)	0.499	0.692	0.548
	Model_3	0.604 (0.547, 0.659)	0.654 (0.593, 0.715)	0.469	0.717	0.532
	Model_4	0.588 (0.530, 0.643)	0.631 (0.568, 0.693)*	0.494	0.583	0.590
15–64 years age group						
	Model_1	0.701 (0.680, 0.722)	0.747 (0.724, 0.769)	0.516	0.475	0.826
	Model_2	0.693 (0.672, 0.714)	0.748 (0.726, 0.770)	0.510	0.470	0.816
	Model_3	0.687 (0.666, 0.708)	0.731 (0.708, 0.753)*	0.484	0.502	0.790
	Model_4	0.650 (0.628, 0.671)	0.679 (0.654, 0.704)*	0.463	0.426	0.773
$\geq 65$ years age group						
	Model_1	0.711 (0.629, 0.784)	0.791 (0.719, 0.864)*	0.531	0.656	0.756
	Model_2	0.704 (0.622, 0.778)	0.750 (0.669, 0.830)*	0.502	0.641	0.756
	Model_3	0.578 (0.492, 0.660)	0.719 (0.635, 0.803)*	0.570	0.422	0.705
	Model_4	0.542 (0.457, 0.626)	0.600 (0.507, 0.693)*	0.531	0.484	0.590

Note: Model\_1 included two epidemiological characteristics and other important variables.

Model\_2 included visiting during a specific week of epidemic season and other important variables.

Model\_3 included visiting during the epidemic season and other important variables.

Model\_4 included important variables except epidemiological characteristics.

Abbreviation: CI=confidence interval.

\* The difference between this model and others was statistically significant in the same group ( $P < 0.05$ ).

<sup>†</sup> The maximum Youden index was used to determine the optimal threshold for influenza prediction.

Based on the most significant symptoms and signs positively associated with influenza (indicated by higher importance value with a positive SHAP value) in the optimal model for the total population, a new ILI definition was developed. The diagnostic performance of the new definition alongside existing WHO, China CDC, and USA CDC ILI definitions was evaluated using the testing dataset. Additionally, cross-correlation analysis of time series between ILI cases under these definitions and confirmed influenza cases was conducted using the cross-correlation function from the Stats package.

All statistical analyses were performed using R software version 4.3.2 (R foundation, Vienna, Austria). Continuous variables were compared using t-tests or Kruskal-Wallis tests as appropriate. Categorical variables were analyzed using chi-squared tests or Fisher's exact tests. The pROC package was employed to determine the optimal body temperature cut-off value (maximum Youden index) and compare model AUC values using the DeLong method.

After data extraction and processing, we established a comprehensive database comprising 200,135 cases. The CongRong model demonstrated exceptional performance in symptom variable extraction, achieving an accuracy of 0.997, sensitivity of 0.991, and specificity of 0.998 in the testing dataset (Supplementary Table S2, available at <https://weekly.chinacdc.cn/>). From the influenza sub-dataset used for developing and validating infection prediction models ( $n=11,753$ ; Supplementary Figure S1), we identified 4,249 (36.2%) influenza-positive cases in the total

population, with positivity rates of 41.6%, 34.9%, and 41.5% in the 0–14 years, 15–64 years, and  $\geq 65$  years age groups, respectively (Supplementary Table S1).

The Boruta algorithm identified distinct sets of important candidate variables for modeling: 18 for the total population, and 7, 16, and 8 variables for the 0–14 years, 15–64 years, and  $\geq 65$  years age groups, respectively (Figure 1). The predictive performance metrics of all 16 machine learning models are presented in Table 1. For the total population, model\_1 emerged as the optimal prediction model, achieving an accuracy of 0.689 (0.669, 0.772) and an AUC of 0.734 (0.710, 0.750). The most influential predictors in this model included body temperature, age, visiting during the epidemic season, visiting during a certain week of epidemic season, cough, and rhinorrhea, with all factors except age showing strong positive associations with influenza (Figure 1). In the 0–14 years age group, model\_1 performed optimally, with body temperature, visiting during a certain week of epidemic season, rhinorrhea, visiting during epidemic season, and cough emerge as the most significant predictors, all demonstrating strong positive correlations with influenza (Figure 1). For the 15–64 years age group, model\_2 proved most effective, with body temperature, visiting during a certain week of epidemic season, age, cough, and rhinorrhea identified as key predictor, all except age showing strong positive associations with influenza (Figure 1). In the  $\geq 65$  years age group, model\_1 demonstrated optimal performance, with visiting during epidemic season, visiting during a certain week of epidemic season, body

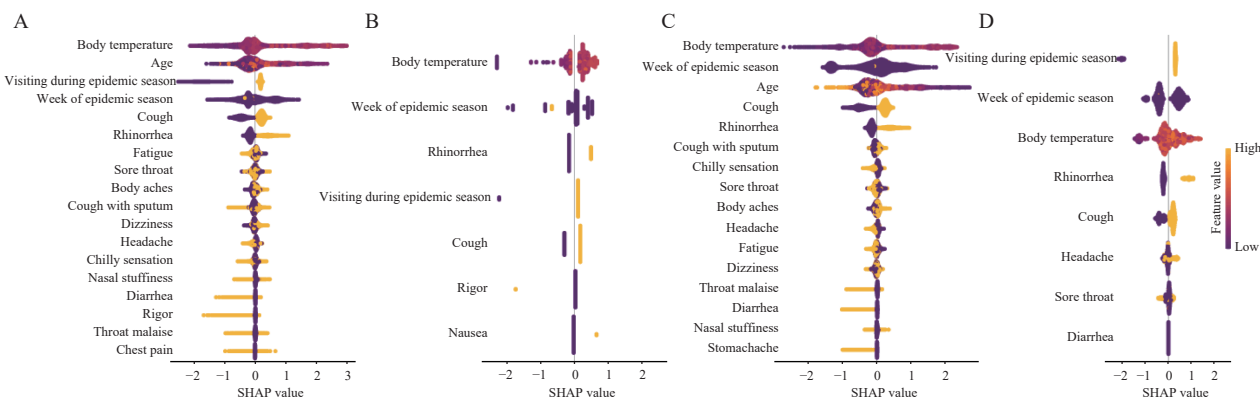


FIGURE 1. SHAP summary plot illustrating variable importance and directional relationships obtained from the optimal model for influenza prediction across the (A) total population, (B) 0–14 years group, (C) 15–64 years group, and (D)  $\geq 65$  years group.

Note: Variables with higher importance values (yellow) and positive SHAP values (right side) demonstrate positive associations, while those with higher importance values (yellow) and negative SHAP values (left side) indicate negative associations.

Abbreviation: SHAP=SHapley Additive exPlanations.

temperature, rhinorrhea, and cough emerging as the most important predictors, all showing strong positive correlations with influenza (Figure 1). The complete performance metrics for both testing and training datasets are detailed in Table 1 and Supplementary Table S3 (available at <https://weekly.chinacdc.cn/>), respectively.

Based on the most important symptoms and signs positively associated with influenza in the optimal model for the total population — body temperature, cough, and rhinorrhea — and using the identified cut-off value for body temperature of 37.9 °C, a new ILI definition was established: fever ( $\geq 37.9$  °C) with either cough or rhinorrhea. This new definition significantly outperformed ( $P < 0.001$ ) the existing WHO, China CDC, and USA CDC definitions in diagnosing influenza, achieving an AUC of 0.618 (0.598, 0.639), accuracy of 0.605 (0.585, 0.625), sensitivity of 0.665, and specificity of 0.572 (Table 2). Time series analyses of ILI cases under the new, WHO, China CDC, and USA CDC definitions alongside confirmed influenza cases during the study period, revealed that the daily trend cross-correlation coefficients between ILI cases under the new, WHO, China CDC, and USA CDC definitions and influenza cases were 0.701 ( $P < 0.05$ ), 0.685 ( $P < 0.05$ ), 0.648 ( $P < 0.05$ ), and 0.653 ( $P < 0.05$ ) respectively, with peak correlations occurring simultaneously.

## DISCUSSION

This study developed machine learning models for influenza prediction using data from three large sentinel hospitals in Chongqing, China, and identified an optimal model with the highest AUC. Based on the model's top three predictive symptoms (fever, cough, and rhinorrhea), a new ILI definition was proposed that demonstrated superior performance compared to existing WHO, China CDC, and USA CDC definitions. Our findings suggest that body temperature, cough, and rhinorrhea serve as crucial

indicators for both early clinical diagnosis of influenza and ILI surveillance.

Our study employed XGBOOST, an advanced machine learning algorithm that has demonstrated superior performance in clinical and epidemiological studies compared to other approaches such as Ranger, Random Forest, Cforest, SVM, Artificial Neural Network, and Deep Learning (5–6). The SHAP value analysis of our optimal models revealed consistent important variables across all age subgroups and the total population, including epidemic season timing, body temperature, cough, and rhinorrhea, aligning with previous research findings (5,7–9). These results underscore two critical points: first, the importance of timely reporting of influenza epidemic trends by national and regional CDC authorities based on surveillance data; and second, the primary clinical indicators — body temperature, cough, and rhinorrhea — that clinicians should prioritize when diagnosing influenza during epidemic seasons.

While ILI definitions vary across countries and WHO revised its definition in 2011 (9), our study aimed to establish a more accurate definition. Based on our optimal prediction model's identification of body temperature, cough, and rhinorrhea as the most significant positive predictors of influenza, with a body temperature threshold of 37.9 °C, we proposed defining ILI as fever ( $\geq 37.9$  °C) with either cough or rhinorrhea. This new definition not only outperformed WHO, China CDC, and USA CDC definitions in our study but also showed the highest daily trend cross-correlation coefficient with confirmed influenza cases. Our temperature threshold of 37.9 °C closely approximates the 38.0 °C specified by WHO and China CDC, and the 37.8 °C by USA CDC. While our definition shares the core elements of fever and cough with existing definitions, it notably substitutes rhinorrhea for sore throat as an alternative criterion. This modification is supported by previous studies identifying rhinorrhea as a common influenza symptom occurring alongside cough (10–11), providing evidence-based justification for optimizing

TABLE 2. Performance of ILIs with the new, WHO, China CDC and USA CDC definitions in predicting influenza.

ILI	AUC (95% CI)	Accuracy (95% CI)	Sensitivity	Specificity
New ILI	0.618 (0.598, 0.639)*	0.605 (0.585, 0.625)	0.665	0.572
WHO ILI	0.599 (0.578, 0.620)	0.602 (0.583, 0.622)	0.587	0.611
China CDC ILI	0.592 (0.572, 0.613)	0.572 (0.551, 0.591)	0.661	0.522
USA CDC ILI	0.592 (0.571, 0.612)	0.560 (0.540, 0.580)	0.701	0.482

Abbreviation: ILI=influenza-like illness; CI=confidence interval; WHO=World Health Organization; AUC=area under curve.

\* The difference in AUC between the new ILI definition and other definitions was statistically significant ( $P < 0.001$ ).

the ILI definition.

Our study has two primary limitations. First, its retrospective design may introduce inherent biases. Second, despite including multiple centers, the data remains geographically confined to one region. Future research should incorporate data from diverse regions and countries to validate these findings.

**Conflicts of interest:** No conflicts of interest.

**Acknowledgments:** Cloudwalk Technology for providing artificial intelligence data processing support.

**Ethical statement:** Received approval from the Research Ethics Board of The First Affiliated Hospital of Chongqing Medical University (approval number: K2024-171-01), with informed consent obtained from all participants.

**Funding:** Supported by the Chongqing Social Science Planning Project (Grant Number 2020PY48) funded by the Chongqing Federation of Social Science and the Joint Project of Chongqing Science and Technology Bureau and Health Commission (Grant Number 2020NCPZX03) funded by the Chongqing Science and Technology Bureau and Chongqing Health Commission of China.

doi: 10.46234/ccdcw2025.059

# Corresponding author: Guangzhao Yi, 202774@hospital.cqmu.edu.cn.

<sup>1</sup> The First Affiliated Hospital of Chongqing Medical University, Chongqing, China; <sup>2</sup> Chongqing Medical University, Chongqing, China; <sup>3</sup> Chongqing Center for Disease Control and Prevention, Chongqing, China; <sup>4</sup> Cloudwalk Technology, Chongqing, China; <sup>5</sup> People's Hospital of Chongqing Banan District, Chongqing, China; <sup>6</sup> The Affiliated Yongchuan Hospital of Chongqing Medical University, Chongqing, China.

<sup>8c</sup> Joint first authors.

Copyright © 2025 by Chinese Center for Disease Control and Prevention. All content is distributed under a Creative Commons Attribution Non Commercial License 4.0 (CC BY-NC).

Submitted: July 12, 2024

Accepted: January 27, 2025

Issued: March 14, 2025

## REFERENCES

- Hartman L, Zhu YW, Edwards KM, Griffin MR, Talbot HK. Underdiagnosis of influenza virus infection in hospitalized older adults. *J Am Geriatr Soc* 2018;66(3):467 – 72. <https://doi.org/10.1111/jgs.15298>.
- González-Bandala DA, Cuevas-Tello JC, Noyola DE, Comas-García A, García-Sepúlveda CA. Computational forecasting methodology for acute respiratory infectious disease dynamics. *Int J Environ Res Public Health* 2020;17(12):4540. <https://doi.org/10.3390/ijerph17124540>.
- World Health Organization. Global influenza surveillance and response system (GISRS). <https://www.who.int/initiatives/global-influenza-surveillance-and-response-system>. [2024-4-28].
- National Health Commission of the People's Republic of China. Diagnosis and treatment scheme for influenza (2020 revised edition) <http://www.nhc.gov.cn/cms-search/downloadFiles/a671529d4c7b428b88489f71212df083.pdf>. [2020-11-4]. (In Chinese).
- Hung SK, Wu CC, Singh A, Li JH, Lee C, Chou EH, et al. Developing and validating clinical features-based machine learning algorithms to predict influenza infection in influenza-like illness patients. *Biomed J* 2023;46(5):100561. <https://doi.org/10.1016/j.bj.2022.09.002>.
- Cheng HY, Wu YC, Lin MH, Liu YL, Tsai YY, Wu JH, et al. Applying machine learning models with an ensemble approach for accurate real-time influenza forecasting in Taiwan: development and validation study. *J Med Internet Res* 2020;22(8):e15394. <https://doi.org/10.2196/15394>.
- Li PF, Wang YN, Peppelenbosch MP, Ma ZR, Pan QW. Systematically comparing COVID-19 with the 2009 influenza pandemic for hospitalized patients. *Int J Infect Dis* 2021;102:375 – 80. <https://doi.org/10.1016/j.ijid.2020.11.127>.
- Morens DM, Taubenberger JK, Fauci AS. A centenary tale of two pandemics: the 1918 influenza pandemic and COVID-19, part I. *Am J Public Health* 2021;111(6):1086 – 94. <https://doi.org/10.2105/AJPH.2021.306310>.
- Fitzner J, Qasmieh S, Mounts AW, Alexander B, Besselaar T, Briand S, et al. Revision of clinical case definitions: influenza-like illness and severe acute respiratory infection. *Bull World Health Organ* 2018; 96(2):122 – 8. <https://doi.org/10.2471/BLT.17.194514>.
- Monto AS, Gravenstein S, Elliott M, Colopy M, Schweinle J. Clinical signs and symptoms predicting influenza infection. *Arch Intern Med* 2000;160(21):3243 – 7. <https://doi.org/10.1001/archinte.160.21.3243>.
- Dugas AF, Hsieh YH, LoVecchio F, Moran GJ, Steele MT, Talan DA, et al. Derivation and validation of a clinical decision guideline for influenza testing in 4 US emergency departments. *Clin Infect Dis* 2020;70(1):49 – 58. <https://doi.org/10.1093/cid/ciz171>.

## SUPPLEMENTARY MATERIALS

### Introduction to Participating Hospitals in this Study

The three hospitals are sentinel hospitals for influenza surveillance, located in the central, southern and western Chongqing, with 3,200, 1,500 and 1,200 beds, respectively; during the study, the number of visits in the emergency department was 27,262, 83,828 and 64,075, and the number of visits in the fever clinic was 16,303, 17,500 and 11,293, respectively.

### Introduction of AI Assistant CongRong and Symptom Variables Extraction Process

As an AI assistant, CongRong is a pre-trained large language model with balanced capabilities in both Chinese and English. It is a transformer-based autoregressive model with 75 billion parameters, with a basic architecture similar to that of a new generation of open source large model, LLama 2. Regarding pre-training data, approximately 55% of data is consistent with that of LLama 2, primarily in English, comprising wiki, arXiv papers, code, e-books, and web content. The remaining 45% is primarily in Chinese, including Chinese encyclopedias, e-books, papers, and web content. CongRong's training ultimately consumed 1.5TB of tokenized pre-training data.

Data for the variables except body temperature were extracted from chief complaint, history of present illness and physical examination within the raw data by CongRong, an artificial intelligence (AI) assistant and pre-trained large language model, to obtain a database for analysis. In order to enable CongRong to better understand the unique expressions and professional terminology specific to this extraction task, we selected a sample dataset with 1,167 cases from the raw data to train and validate CongRong model: first, three clinicians read the medical records of the sample cases and recorded whether a patient exhibited any of the 26 symptoms (annotated positive 1 and negative 0); then the sample dataset was divided into a training dataset ( $n=854$ ) and a testing dataset ( $n=313$ ), and the training dataset was used to fine-tune the CongRong pre-trained model; finally, the CongRong pre-trained model was validated in the testing dataset.

### The Definitions Involved in this Study

**Epidemic season for influenza** The start of an epidemic season was defined as the first week during which the infection (influenza) positive rate was higher than the average infection positive rate for the study period (a surveillance year) and remained above that level for at least four consecutive weeks; the end of an epidemic season was defined as the first week during which the infection (influenza) positive rate was lower than the average infection positive rate for the study period and remained below that level for at least four consecutive weeks (1,2).

We collected two epidemiological characteristics variables included visiting during respective epidemic season of influenza and visiting during a certain week of epidemic season. According to the definition of epidemic season, we determined that the study period included two influenza seasons with a total of 12 weeks.

**Influenza-like illness defined by WHO** An acute respiratory illness with a measured temperature of  $\geq 38^{\circ}\text{C}$  and cough, with onset within the past 10 days (3).

**Influenza-like illness defined by China CDC** Fever ( $\geq 38.0^{\circ}\text{C}$ ) with cough or sore throat (4).

**Influenza-like illness defined by USA CDC** Fever ( $\geq 37.8^{\circ}\text{C}$ ) and a cough and/or a sore throat (5).

SUPPLEMENTARY TABLE S1. Characteristics of patients undergoing influenza laboratory testing.

Variables	Total		0–14 years group		15–64 years group		≥65 years group		
	Total	Influenza	Influenza	Influenza	Influenza	Influenza	Influenza	Influenza	
	(N=11,753)	negative	positive	negative	positive	negative	positive	negative	positive
	(N=7,504)	(N=4,249)	(N=901)	(N=641)	(N=6,187)	(N=3,313)	(N=416)	(N=295)	
Age, years, median (IQR)	25 (17–36)	25 (17–35)	26 (17–36)	8 (4–14)	6 (3–14)*	26 (19–35)	27 (20–36)*	73 (68–78)	73 (69–80)
Female	6,079 (51.7)	3,988 (53.1)	2,091 (49.2)*	430 (47.7)	280 (43.7)	3,347 (54.1)	1,676 (50.6)*	211 (50.7)	135 (45.8)
Visiting during epidemic season, n (%)	10,006 (85.1)	5,906 (78.7)	4,100 (96.5)*	808 (89.7)	631 (98.4)*	4,818 (77.9)	3,181 (96.0)*	280 (67.3)	288 (97.6)*
Visiting during a certain week of epidemic season, n (%)									
The first influenza season									
1	96 (0.8)	59 (0.8)	37 (0.9)*	35 (3.9)	16 (2.5)*	23 (0.4)	17 (0.5)*	1 (0.2)	4 (1.4)*
2	935 (8.0)	395 (5.3)	540 (12.7)	68 (7.5)	91 (14.2)	280 (4.5)	380 (11.5)	47 (11.3)	69 (23.4)
3	1,209 (10.3)	509 (6.8)	700 (16.5)	111 (12.3)	158 (24.6)	350 (5.7)	454 (13.7)	48 (11.5)	88 (29.8)
4	862 (7.3)	451 (6.0)	411 (9.7)	139 (15.4)	141 (22.0)	270 (4.4)	237 (7.2)	42 (10.1)	33 (11.2)
5	335 (2.9)	229 (3.1)	106 (2.5)	71 (7.9)	32 (5.0)	143 (2.3)	63 (1.9)	15 (3.6)	11 (3.7)
The second influenza season									
1	336 (2.9)	220 (2.9)	116 (2.7)	22 (2.4)	20 (3.1)	194 (3.1)	94 (2.8)	4 (1.0)	2 (0.7)
2	1,121 (9.5)	728 (9.7)	393 (9.2)	77 (8.5)	56 (8.7)	640 (10.3)	332 (10.0)	11 (2.6)	5 (1.7)
3	1,521 (12.9)	933 (12.4)	588 (13.8)	117 (13.0)	61 (9.5)	795 (12.8)	511 (15.4)	21 (5.0)	16 (5.4)
4	1,298 (11.0)	787 (10.5)	511 (12.0)	76 (8.4)	39 (6.1)	684 (11.1)	446 (13.5)	27 (6.5)	26 (8.8)
5	1,086 (9.2)	742 (9.9)	344 (8.1)	59 (6.5)	9 (1.4)	658 (10.6)	322 (9.7)	25 (6.0)	13 (4.4)
6	787 (6.7)	546 (7.3)	241 (5.7)	21 (2.3)	8 (1.2)	497 (8.0)	222 (6.7)	28 (6.7)	11 (3.7)
7	420 (3.6)	307 (4.1)	113 (2.7)	12 (1.3)	0 (0)	284 (4.6)	103 (3.1)	11 (2.6)	10 (3.4)
Symptoms and signs, n (%)									
Body temperature, °C, mean±SD	38.3±0.9	38.2±1.0	38.5±0.8*	38.5±1.0	38.9±0.8*	38.2±1.0	38.5±0.8*	38.1±1.0	38.3±0.8*
Body aches	5,243 (44.6)	3,247 (43.3)	1,996 (47.0)*	144 (16.0)	89 (13.9)	2,960 (47.8)	1,796 (54.2)*	143 (34.4)	111 (37.6)
Fatigue	4,970 (42.3)	3,096 (41.3)	1,874 (44.1)*	145 (16.1)	102 (15.9)	2,774 (44.8)	1,634 (49.3)*	177 (42.5)	138 (46.8)
Chilly sensation	3,712 (31.6)	2,351 (31.3)	1,361 (32.0)	118 (13.1)	75 (11.7)	2,104 (34.0)	1,197 (36.1)*	129 (31.0)	89 (30.2)
Rigor	308 (2.6)	227 (3.0)	81 (1.9)*	23 (2.6)	7 (1.1)	180 (2.9)	66 (2.0)*	24 (5.8)	8 (2.7)
Sleepiness	14 (0.1)	9 (0.1)	5 (0.1)*	0 (0)	0 (0)	5 (0.1)	3 (0.1)	4 (1.0)	2 (0.7)
Headache	4,037 (34.3)	2,474 (33.0)	1,563 (36.8)*	131 (14.5)	97 (15.1)	2,242 (36.2)	1,371 (41.4)*	101 (24.3)	95 (32.2)*
Dizziness	4,605 (39.2)	2,799 (37.3)	1,806 (42.5)*	191 (21.2)	139 (21.7)	2,478 (40.1)	1,547 (46.7)*	130 (31.3)	120 (40.7)*
Cough	7,236 (61.6)	4,055 (54.0)	3,181 (74.9)*	504 (55.9)	436 (68.0)*	3,320 (53.7)	2,525 (76.2)*	231 (55.5)	220 (74.6)*
Cough with sputum	3,967 (33.8)	2,218 (29.6)	1,749 (41.2)*	190 (21.1)	122 (19.0)	1,870 (30.2)	1,468 (44.3)*	158 (38.0)	159 (53.9)*
Sore throat	5,270 (44.8)	3,206 (42.7)	2,064 (48.6)*	200 (22.2)	138 (21.5)	2,921 (47.2)	1,829 (55.2)	85 (20.4)	97 (32.9)*
Throat malaise†	646 (5.5)	423 (5.6)	223 (5.2)*	12 (1.3)	10 (1.6)	393 (6.4)	198 (6.0)	18 (4.3)	15 (5.1)
Rhinorrhea	2,946 (25.1)	1,523 (20.3)	1,423 (33.5)*	176 (19.5)	198 (30.9)*	1,289 (20.8)	1,139 (34.4)*	58 (13.9)	86 (29.2)*

Continued

Variables	Total (N=11,753)	Total		0–14 years group		15–64 years group		≥65 years group	
		Influenza negative	Influenza positive	Influenza negative	Influenza positive	Influenza negative	Influenza positive	Influenza negative	Influenza positive
		(N=7,504)	(N=4,249)	(N=901)	(N=641)	(N=6,187)	(N=3,313)	(N=416)	(N=295)
Nasal stuffiness	1149 (9.8)	702 (9.4)	447 (10.5)*	89 (9.9)	57 (8.9)	597 (9.6)	374 (11.3)*	16 (3.8)	16 (5.4)
Hemoptysis	7 (0.1)	5 (0.1)	2 (0.05)	0 (0)	0 (0)	3 (0.05)	1 (0.03)	2 (0.5)	1 (0.3)
Chest pain	231 (2.0)	135 (1.8)	96 (2.3)	6 (0.7)	1 (0.2)	118 (1.9)	83 (2.5)	11 (2.6)	12 (4.1)
Shortness of breath	195 (1.7)	121 (1.6)	74 (1.7)	3 (0.3)	1 (0.2)	94 (1.5)	48 (1.4)	24 (5.8)	25 (8.5)
Dyspnea	91 (0.8)	54 (0.7)	37 (0.9)	0 (0)	0 (0)	40 (0.6)	31 (0.9)	14 (3.4)	6 (2.0)
Palpitation	198 (1.7)	135 (1.8)	63 (1.5)	2 (0.2)	4 (0.6)	115 (1.9)	51 (1.5)	18 (4.3)	8 (2.7)
Diarrhea	397 (3.4)	304 (4.1)	93 (2.2)*	14 (1.6)	6 (0.9)	268 (4.3)	79 (2.4)*	22 (5.3)	8 (2.7)
Stomachache	265 (2.3)	195 (2.6)	70 (1.6)*	34 (3.8)	27 (4.2)	144 (2.3)	38 (1.1)*	17 (4.1)	5 (1.7)
Nausea	811 (6.9)	515 (6.9)	296 (7.0)	22 (2.4)	32 (5.0)*	457 (7.4)	238 (7.2)	36 (8.7)	26 (8.8)
Vomiting	585 (5.0)	389 (5.2)	196 (4.6)	56 (6.2)	42 (6.6)	297 (4.8)	126 (3.8)*	36 (8.7)	28 (9.5)
Conjunctivitis	3 (0.03)	3 (0.04)	0 (0)	0 (0)	0 (0)	3 (0.05)	0 (0)	0 (0)	0 (0)
Impaired sense of smell	4 (0.03)	4 (0.1)	0 (0)	0 (0)	0 (0)	2 (0.03)	0 (0)	2 (0.5)	0 (0)
Impaired taste	16 (0.1)	14 (0.2)	2 (0.05)	0 (0)	0 (0)	13 (0.2)	1 (0.03)	1 (0.2)	1 (0.3)
Rash	42 (0.4)	32 (0.4)	10 (0.2)	6 (0.7)	3 (0.5)	23 (0.4)	7 (0.2)	3 (0.7)	0 (0)

Abbreviation: IQR=interquartile range; SD=standard deviation.

\* The difference between influenza-positive and -negative cases was statistically significant ( $P<0.05$ ).

† Pharyngeal discomfort included feelings of dryness, itching, and other discomfort in the throat, excluding sore throat.

SUPPLEMENTARY TABLE S2. The performance of CongRong pre-trained model in this study.

Symptoms	Accuracy	Sensitivity	Specificity
Body aches	0.997	1.000	0.996
Fatigue	0.997	0.987	1.000
Chills	0.994	1.000	0.993
Rigor	1.000	1.000	1.000
Somnolence	1.000	–	1.000
Headache	0.994	0.985	0.996
Dizziness	1.000	1.000	1.000
Cough	0.994	0.991	0.995
Expectoration	1.000	1.000	1.000
Sore throat	1.000	1.000	1.000
Pharyngeal discomfort	0.997	1.000	0.997
Rhinorrhea	0.994	0.949	1.000
Nasal congestion	1.000	1.000	1.000
Hemoptysis	1.000	1.000	1.000
Chest pain	1.000	1.000	1.000
Shortness of breath	0.994	1.000	0.993
Dyspnea	1.000	1.000	1.008
Palpitation	1.000	1.000	1.000
Diarrhea	0.997	1.000	0.997
Abdominal pain	0.994	1.000	0.993
Nausea	0.997	1.000	0.997
Vomiting	0.994	0.931	1.000
Conjunctivitis	1.000	1.000	1.000
Impaired sense of smell	1.000	1.000	1.000
Impaired taste	0.997	1.000	0.997
Erythra	1.000	1.000	1.000
Total	0.997	0.991	0.998

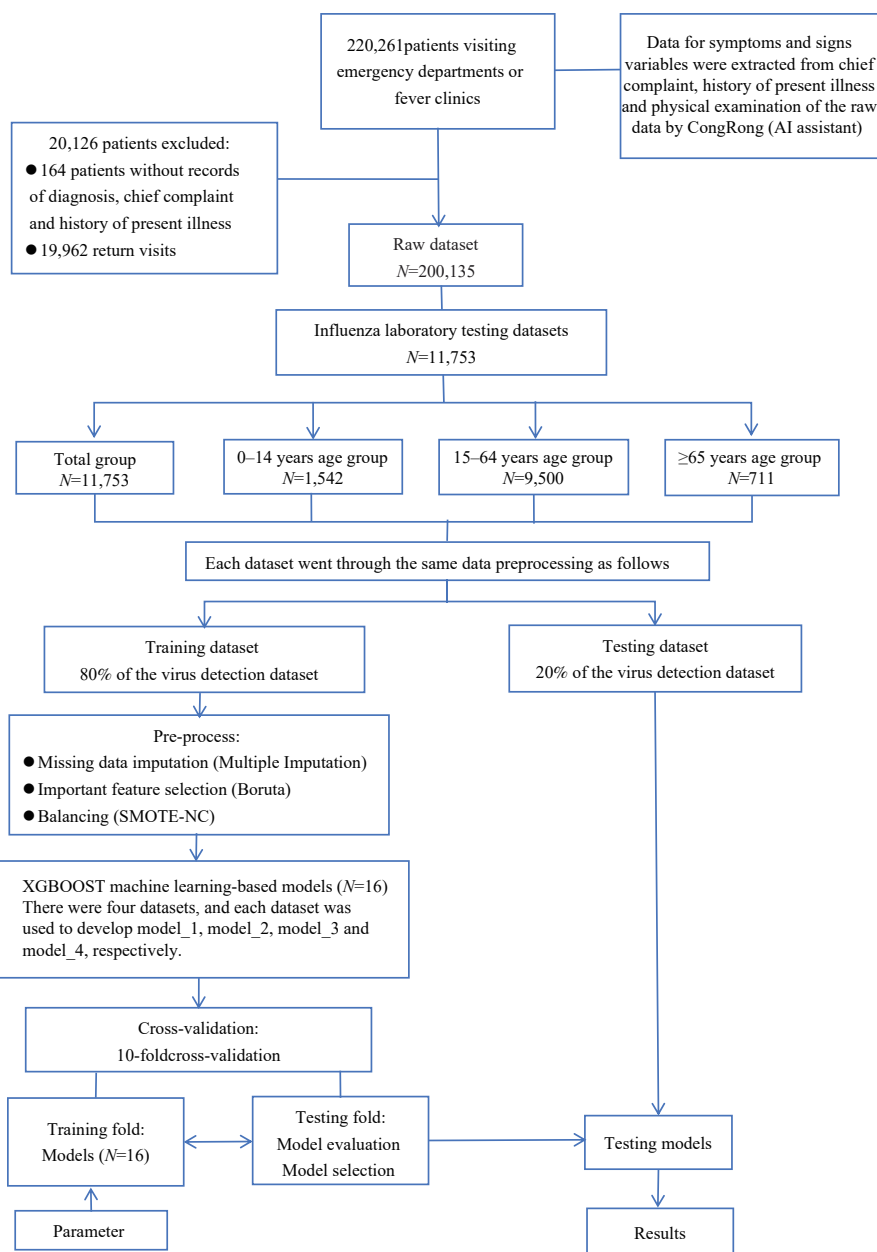
Note: –: There were no patients with positive somnolence in the model training set.

SUPPLEMENTARY TABLE S3. Performance of machine learning-based prediction models for influenza in the training dataset.

Dataset	Models	Accuracy (95% CI)	AUC (95% CI)	Threshold*	Sensitivity	Specificity
Total population	Model_1	0.841 (0.835, 0.848)	0.926 (0.922, 0.931)	0.500	0.833	0.849
	Model_2	0.856 (0.849, 0.862)	0.934 (0.930, 0.938)	0.486	0.845	0.867
	Model_3	0.795 (0.787, 0.802)	0.890 (0.884, 0.895)	0.496	0.778	0.812
	Model_4	0.826 (0.820, 0.833)	0.910 (0.905, 0.915)	0.483	0.798	0.855
0–14 years age group	Model_1	0.703 (0.678, 0.726)	0.762 (0.738, 0.787)	0.500	0.794	0.612
	Model_2	0.700 (0.675, 0.724)	0.762 (0.738, 0.787)	0.499	0.787	0.613
	Model_3	0.692 (0.668, 0.716)	0.780 (0.757, 0.803)	0.469	0.798	0.586
	Model_4	0.671 (0.646, 0.696)	0.742 (0.717, 0.767)	0.494	0.698	0.644
15–64 years age group	Model_1	0.838 (0.831, 0.845)	0.923 (0.918, 0.928)	0.516	0.793	0.883
	Model_2	0.828 (0.820, 0.835)	0.911 (0.905, 0.916)	0.510	0.786	0.869
	Model_3	0.807 (0.799, 0.815)	0.897 (0.891, 0.903)	0.484	0.790	0.823
	Model_4	0.813 (0.805, 0.820)	0.898 (0.892, 0.904)	0.463	0.786	0.839
≥65 years age group	Model_1	0.778 (0.745, 0.809)	0.848 (0.820, 0.877)	0.531	0.793	0.763
	Model_2	0.802 (0.770, 0.831)	0.871 (0.844, 0.897)	0.502	0.802	0.802
	Model_3	0.836 (0.806, 0.863)	0.924 (0.906, 0.942)	0.570	0.817	0.855
	Model_4	0.772 (0.739, 0.803)	0.860 (0.833, 0.887)	0.470	0.784	0.760

Abbreviation: CI=confidence interval.

\* The maximum Youden index was used to determine the optimal threshold for influenza prediction.



SUPPLEMENTARY FIGURE S1. Flow chart for patient enrollment, dataset establishment, and statistical analysis of prediction models for influenza in this study.

Note: Data preprocessing: the sub-dataset for developing and validating the influenza prediction models consisted of data from cases that underwent influenza laboratory testing. First, the sub-dataset was randomly partitioned into an 80% training dataset and a 20% testing dataset, stratified by infection status. Second, missing values in the training dataset were imputed using multiple imputation via the Mice package. Third, the training dataset was used to extract important candidate variables and remove unimportant variables using the Boruta algorithm. Finally, the data were balanced using the synthetic minority oversampling technique for nominal and continuous algorithm via the Themis package. Machine learning-based modeling: after data preprocessing, we developed four candidate models on each training dataset of the total population and three age subgroups (0–14 years, 15–64 years, and ≥65 years) to predict influenza. The independent variables included in the four models were combinations of two epidemiological characteristics variables and other important variables extracted by the Boruta algorithm. We performed ten-fold cross-validations to tune the parameters using the Caret package and developed machine learning-based models on each training dataset using XGBOOST algorithm. Model\_1 included two epidemiological characteristics and other important variables. Model\_2 included visiting during a certain week of epidemic season and other important variables. Model\_3 included visiting during epidemic season and other important variables. Model\_4 included important variables except epidemiological characteristics.

Abbreviation: AI=artificial intelligence; SMOTE-NC=Synthetic Minority Oversampling Technique for Nominal and Continuous.

## REFERENCES

1. Azziz Baumgartner E, Dao CN, Nasreen S, Bhuiyan MU, Mah-E-muneer S, Mamun AA, et al. Seasonality, timing, and climate drivers of influenza activity worldwide. *J Infect Dis* 2012;206(6):838 – 46. <https://doi.org/10.1093/infdis/jis467>.
2. Ye CC, Zhu WP, Yu JX, Li ZJ, Zhang YZ, Wang YP, et al. Understanding the complex seasonality of seasonal influenza A and B virus transmission: evidence from six years of surveillance data in Shanghai, China. *Int J Infect Dis* 2019;81:57 – 65. <https://doi.org/10.1016/j.ijid.2019.01.027>.
3. Fitzner J, Qasmieh S, Mounst AW, Alexander B, Besselaar T, Briand S, et al. Revision of clinical case definitions: influenza-like illness and severe acute respiratory infection. *Bull World Health Organ* 2018;96(2):122 – 8. <https://doi.org/10.2471/BLT.17.194514>.
4. National Health Commission of the People's Republic of China. National influenza surveillance program (2017 version). <http://www.nhc.gov.cn/jkj/s3577/201704/ed1498d9e64144738cc7f8db61a39506.shtml>. [2017-4-2]. (In Chinese).
5. Centers for Disease Control and Prevention. U.S. influenza surveillance: purpose and methods. [https://www.cdc.gov/fluview/overview/?CDC\\_AAref\\_Val](https://www.cdc.gov/fluview/overview/?CDC_AAref_Val). [2023-11-5].

## Preplanned Studies

## Infodemic Management and Public Health Emergency Preparedness Capacities — Khyber Pakhtunkhwa, Pakistan, 2024

Majid Ali Tahir<sup>1,2</sup>; Ijaz ul Haq<sup>1,3,4,\*</sup>; Shahbaz Ahmad Zakki<sup>1</sup>; Fazli Akbar<sup>5</sup>

### Summary

#### What is already known about this topic?

The infodemics can increase the burden of outbreaks and emergencies. Many of the studies documented the impact and emergence of the infodemic situation during epidemics or pandemics in recent years. There is limited evidence on the preparedness and readiness of health departments to effectively manage the infodemic situation.

#### What is added by this report?

This research provides a comprehensive assessment of the health department's capabilities in crisis emergency risk communication and infodemic management, identifying key best practices, challenges and bottlenecks. It contributes to the field by offering a framework and methodologies for evaluating these capacities, aiding in improving infectious diseases outbreak response public health emergency management.

#### What are the implications for public health practice?

Countries and health departments can benefit from these insights by assessing the level of preparedness and readiness in this field and to implement targeted interventions to enhance their preparedness and response capabilities to misinformation and disinformation.

## ABSTRACT

**Introduction:** The spread of misinformation and disinformation during infectious disease outbreaks and public health emergencies can significantly impede effective public health responses. This infodemic phenomenon creates confusion and erodes public trust, leading to uncertainty in crisis situations. This study aimed to assess the health department's capacity and capabilities in infodemic preparedness and management to enhance future emergency

preparedness in accordance with International Health Regulations (IHR)-2005 guidelines.

**Methods:** A mixed-methods cross-sectional study was conducted in the health department of Khyber Pakhtunkhwa. Semi-structured interviews with experts were conducted in August-September 2024 using a self-administered assessment tool based on IHR-2005 guidelines, supplemented by analysis of departmental documents and supporting evidence. Data were analyzed using descriptive statistics, with achievement levels scored from 0% to 100% across five categories.

**Results:** The overall preparedness score was 21.7%, indicating limited capacities and capabilities. The risk communication and community engagement (RCCE) coordination system showed some strengths, with 80% of focal persons designated and moderate intersectoral coordination (40%), but lacked emergency spokesperson training. Community engagement activities demonstrated moderate effectiveness (40%). Key weaknesses included insufficient human resources (20%), inadequate technological infrastructure (20%), absence of infodemic analysis (0%), and lack of joint infodemic planning (0%). Significant delays were observed in identifying and responding to potentially harmful misinformation.

**Conclusions:** Despite some effective practices in community engagement, substantial gaps exist in infodemic management preparedness. Critical deficiencies were identified in human and technological resources and infodemic response measures. Priority areas for improvement include human resource development, infodemic surveillance systems, digital tools implementation, and enhanced collaboration. The adoption of innovative tools and streamlined processes is essential for strengthening emergency risk communication preparedness.

The spread of misinformation and disinformation

alongside infectious disease outbreaks can significantly impede public health responses. This study assessed the health department's capacity in infodemic management to enhance future emergency response capabilities. A mixed-methods cross-sectional study was conducted in the Khyber Pakhtunkhwa health department using semi-structured expert interviews based on International Health Regulations (IHR)-2005 guidelines, complemented by departmental document review of risk communication capacities. The overall preparedness score was 21.7%, indicating substantial deficiencies in capacities and capabilities. While some strengths were observed in the risk communication and community engagement (RCCE) coordination system, with 80% designated focal persons, intersectoral coordination remained moderate (40%) with notable gaps in emergency spokesperson training. Community engagement activities demonstrated moderate effectiveness (40%). Key weaknesses included limited human resources (20%), limited technological infrastructure (20%), absence of infodemic analysis (0%), and significant delays in identifying and responding to misinformation spread. Despite some effective practices in coordination and community engagement, critical gaps persist in infodemic management preparedness, particularly in human and technological resources and response measures. Priority areas for improvement include human resource development, infodemic surveillance systems, digital tool implementation, and enhanced stakeholder collaboration.

Public health emergencies and disease outbreaks can be significantly exacerbated by the concurrent spread of misinformation and disinformation. While misinformation refers to false information shared without malicious intent, disinformation represents deliberately misleading content. The rapid dissemination of diverse and often contradictory information during outbreaks or emergencies can precipitate an infodemic situation. An infodemic is characterized by an overabundance of information, including false or misleading content, in digital and physical environments during a disease outbreak (1). These infodemics can propagate rapidly and achieve widespread reach, particularly during the initial phases of an epidemic or emergency when official information is limited (2–4). Pakistan's second Joint External Evaluation (JEE) identified substantial gaps in health emergency preparedness, risk communication, and infodemic management systems (5). The Khyber Pakhtunkhwa province, operating under a devolved

health system, lacks a comprehensive risk communication and community engagement plan, though some informal community engagement activities are conducted within the existing primary healthcare framework (5–6). This study represents an effort to assess the capacities within Khyber Pakhtunkhwa to identify best practices, gaps, and challenges. The research aims to identify enablers, bottlenecks, and existing infodemic management capacities to strengthen health department preparedness for future public health crises. Furthermore, the findings and methodological approach will contribute to the evolving field of infodemic management by providing valuable insights for low- and middle-income countries (LMICs) in assessing their risk communication and infodemic response capabilities.

This cross-sectional study was conducted at the Provincial Health Department of Khyber Pakhtunkhwa, Pakistan. A total of 19 subject matter experts (SMEs) were recruited through departmental correspondence, comprising 15 public health experts and 4 additional specialists (Supplementary Table S1, available at <https://weekly.chinacdc.cn/>). These SMEs were nominated by their respective organizations, representing the animal health department, climate change, environment, and information and public relations departments.

Primary data collection occurred from August to September 2024 using a self-administered semi-structured tool based on the Health Emergency Preparedness Self-Assessment (HEPSA) guidelines developed by the European CDC (7). The tool was modified and contextualized to assess RCCE and infodemic capacities as recommended in the IHR Benchmarks 2023 (8). Focus group interviews were conducted at the provincial health department using a peer-to-peer consensus-building approach, as recommended by Joint External Evaluation (4). Additionally, public health planning documents from 2021 onward were reviewed.

Data analysis employed descriptive statistics following the scoring guidelines of the HEPSA tool (7), GHS Index, and CEDM tool developed by New Zealand Ministry of Civil Defense and Emergency Management (9). A percentage-based scoring system was implemented to assess departmental achievement across various progress levels. The scale ranged from “Never” (0%) indicating complete absence of implementation to “Always” (100%) signifying full achievement with sustainable practices. Intermediate

levels included “Infrequently” (20%) for initial stages, “Sometimes” (40%) for partial progress without systematic approach, “Often” (60%) for demonstrated commitment with unclear full attainment, and “Mostly” (80%) for substantial progress with minor limitations (Supplementary Table S2, available at <https://weekly.chinacdc.cn/>). Both descriptive statistical analysis and qualitative thematic analysis were conducted on the primary data and departmental documentation.

The overall score for Risk Communication and Infodemic Management preparedness was 21.7%, indicating significant deficiencies in the health department’s capacity and readiness to manage infodemic situations during large-scale outbreaks and public health emergencies.

As shown in Table 1, the RCCE coordination system demonstrated variable capacity across different domains. The department consistently maintained designated RCCE focal persons with dedicated authority (80% achievement). However, public health spokespersons were appointed only during emergencies and lacked formal RCCE training. Intersectoral coordination operated primarily on an ad hoc basis, achieving moderate capacity (40%). The overall capacity distribution is illustrated in Supplementary Figure S1 (available at <https://weekly.chinacdc.cn/>).

Figure 1 reveals critically limited technological infrastructure for RCCE and infodemic management, with an overall score of 12%. The department’s technological readiness was particularly concerning, with only one training session conducted on

communication channel utilization (Table 1).

The health department’s infodemic analysis and risk assessment capabilities showed significant limitations. While traditional methods were employed for infodemic analysis, achieving a 40% score for rumor verification, sentiment analysis implementation remained minimal at 20%. Only 20% of staff received training in infodemic surveillance and analysis (Figure 1 and Figure 2).

Assessment of the workforce and response system revealed several areas requiring enhancement. Although the department maintains dedicated personnel for risk communication, infodemic surveillance, and community engagement, other metrics indicated substantial weaknesses. Notably, staff training exercises in infodemic surveillance and management were conducted infrequently, achieving only a 20% implementation rate (Figure 1).

Community engagement emerged as a relative strength within the health department’s capabilities. The department maintained a moderate social media community engagement system (40%) and conducted numerous community awareness and engagement sessions. The department demonstrated moderate capacity (40%) in executing community awareness and engagement initiatives, though partnerships with media and other agencies remained primarily informal (Figure 2).

Quantitative assessment revealed that 14 staff members were engaged in community outreach activities, while risk communication activities were supported by only 6 staff members. Response time

TABLE 1. Preparedness capacity scores of Khyber Pakhtunkhwa Health Department for infodemic management.

Sr#	Indicator	Score	Remarks
1	RCCE focal person	80%	RCCE focal person and spokesperson were identified.
2	Infodemic surveillance	20%	Lacks a proper system for online infodemic surveillance and monitoring.
3	Tools for surveillance	0%	No software available for monitoring online information flow.
4	Rumor verification	40%	Somewhat functional rumors verification system in place.
5	Infodemic analysis	0%	Lacks a system for infodemic analysis.
6	Sentiments analyses	20%	Sentiment analysis not being used.
7	Trained staff	20%	Only 2 staff trained on infodemic surveillance and analysis.
8	Social media engagement	40%	Somewhat functional social media community engagement system in place.
9	Active partnerships	20%	Only 3 active partnerships with WHO, UNICEF and Polio EOC.
10	Information sharing	0%	No information sharing meetings or briefings about misinformation or disinformation.
11	Joint planning for infodemic response	0%	No joint action plans for infodemic response.

Note: This table presents the preparedness capacity scores of the Khyber Pakhtunkhwa Health Department for infodemic management. A score of 100% indicates full preparedness, while 0% indicates no preparedness. The “Remarks” column provides contextual explanations for the assigned scores.

Abbreviation: RCCE=risk communication and community engagement.

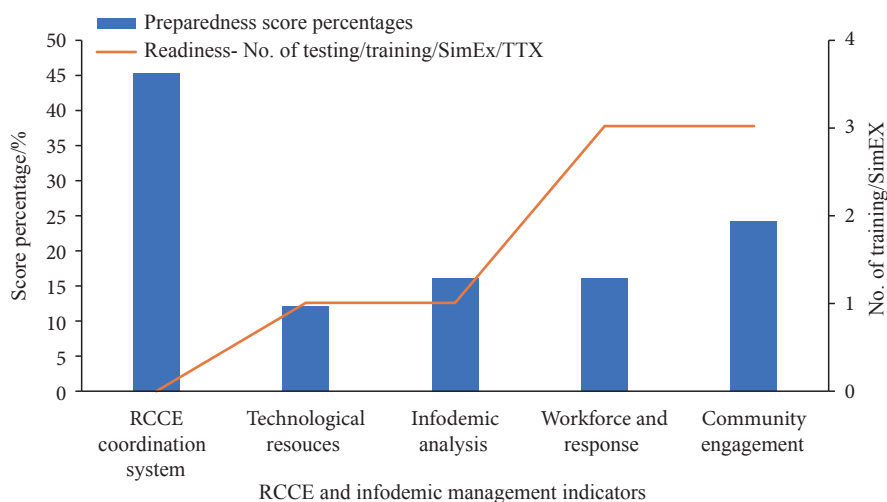


FIGURE 1. Indicator-wise risk communication and community engagement preparedness status of health department in Khyber Pakhtunkhwa.

Note: This bar graph illustrates the preparedness and readiness scores for the Khyber Pakhtunkhwa Health Department across various risk communication and community engagement indicators. The y-axis shows achievement scores as percentages (0–100%), while the x-axis displays the different indicators of risk communication and infodemic management capacities and capabilities.

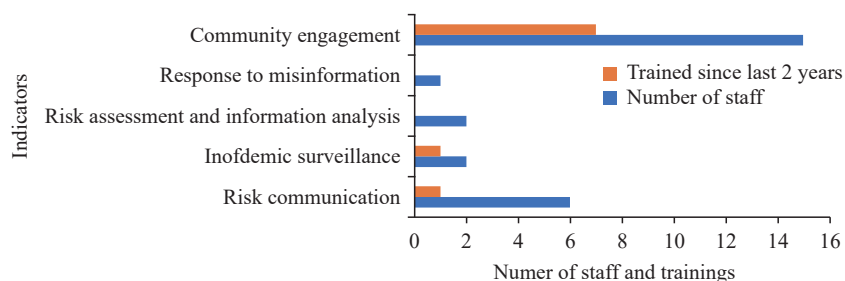


FIGURE 2. Workforce capacity and capability of Khyber Pakhtunkhwa Health Department for infodemic management.

Note: This bar graph depicts the workforce capacity and capabilities of the Khyber Pakhtunkhwa Health Department for infodemic management. The y-axis quantifies staffing levels, capacity building initiatives, and training completion rates, while the x-axis presents key indicators related to workforce competencies and infodemic management practices.

analysis indicated concerning delays: 25 days for dengue-related misinformation detection and 30 days for cholera-related false information response. The department averaged 18.3 days to identify new misinformation threats and 6.6 days to implement responses (Supplementary Figure S2, available at <https://weekly.chinacdc.cn/>).

## DISCUSSION

The findings of our study revealed both strengths and limitations in the Khyber Pakhtunkhwa Health Department's capacity for RCCE and infodemic management. Notable strengths include an established RCCE coordination system, dedicated focal person designation, effective community engagement practices, and demonstrated leadership in crisis

communication. However, significant gaps exist in technological infrastructure, workforce capacity, and infodemic analysis capabilities, indicating lower levels of preparedness. While some training initiatives have been implemented, there are substantial deficiencies in capacity testing, operational training, simulation exercises, and overall responsiveness to managing mis- and disinformation.

Our assessment identified critical challenges in the health department's preparedness for managing misinformation during infectious disease outbreaks and public health emergencies. A key finding was the limited capacity for infodemic surveillance and monitoring, a common challenge among LMICs that have yet to develop systematic monitoring capabilities (1). The department's technological infrastructure for online information monitoring and infodemic analysis

remains inadequate. This observation aligns with research by Donelle et al., who identified insufficient investment in these tools as a significant barrier to effective health communication and emergency response (10).

Our analysis revealed that the health department predominantly relies on traditional methods and lacks adequately trained personnel for information flow monitoring, rumor management, and news verification. Current literature advocates for a paradigm shift toward modern information monitoring and infodemic management approaches, incorporating active social listening and digital analysis tools (11–12). The current situation results in significant delays — averaging 18.3 days for identifying and 6.6 days for responding to new misinformation and disinformation threats — highlighting the urgent need for enhanced workforce development, technological infrastructure, and capacity building. These findings are consistent with Purnat's research emphasizing the critical importance of training health professionals in infodemic management strategies (13).

Community engagement emerged as a relative strength of the health department, demonstrated through effective utilization of social media platforms, community sessions, and strategic partnerships. This aligns with existing literature suggesting that sustained community engagement efforts are crucial for mounting timely responses to future outbreaks (14–15). The implementation of collaborative community engagement approaches can significantly enhance risk communication and infodemic management capabilities for emergency response.

This study's scope was limited to Khyber Pakhtunkhwa, Pakistan, with input from only 19 subject matter experts and no community perspectives, potentially affecting its generalizability to the national level. The findings may not fully represent risk communication capacities across operational and tactical levels.

Our assessment identified critical gaps in infodemic management preparedness, particularly regarding technological resources, infodemic analysis methods, risk assessment protocols, response times, and community information sharing. While the existing RCCE coordination system and community engagement activities provide a valuable foundation, developing a comprehensive infodemic management strategy is essential. We recommend that the health department prioritize investments in enhanced technological infrastructure, implement robust health

infodemic surveillance systems, adopt advanced analytical methods, increase trained personnel, and strengthen risk communication through active stakeholder engagement to effectively manage future public health emergencies.

**Conflicts of interest:** No conflicts of interest.

**Acknowledgement:** The support of leadership and subject matter experts from the Health Department Khyber Pakhtunkhwa, Livestock Department KP, WHO country and provincial office Pakistan, UNICEF Pakistan office, and JSI KP office who participated in the study and shared documentation on preparedness and planning; the Deanship for Scientific Research, King Faisal University, Saudi Arabia for funding support; and the National IHR-2005 Focal Person of Pakistan at NIH for coordinating support of this study.

**Ethical statement:** While this study did not involve human subjects research, as it focused on organizational and institutional preparedness for risk communication, ethical approval was obtained from the Ethics Review Board of the University of Haripur, Khyber Pakhtunkhwa, Pakistan.

**Funding:** Supported by funding from the Deanship for Scientific Research, King Faisal University, Saudi Arabia (KFU250563).

doi: 10.46234/ccdcw2025.060

# Corresponding author: Ijaz ul Haq, [ijazbrt@outlook.com](mailto:ijazbrt@outlook.com).

<sup>1</sup> Department of Public Health & Nutrition, The University of Haripur, Haripur, Khyber Pakhtunkhwa, Pakistan; <sup>2</sup> Center for Disease Control, National Institutes of Health, Islamabad, Pakistan; <sup>3</sup> Department of Clinical Nutrition, King Faisal University, Al-Ahsa, Saudi Arabia; <sup>4</sup> Department of Nursing, Children's Hospital of Fudan University, Shanghai, China; <sup>5</sup> Department of Nutrition and Food Hygiene, School of Public Health, Southern Medical University, Guangzhou City, Guangdong Province, China.

Copyright © 2025 by Chinese Center for Disease Control and Prevention. All content is distributed under a Creative Commons Attribution Non Commercial License 4.0 (CC BY-NC).

Submitted: December 24, 2024

Accepted: March 06, 2025

Issued: March 14, 2025

## REFERENCES

1. Chiou H, Voegeli C, Wilhelm E, Kolis J, Brookmeyer K, Prybylski D. The future of infodemic surveillance as public health surveillance. *Emerg Infect Dis* 2022;28(13):S121 – 8. <https://doi.org/10.3201/eid2813.220696>.
2. Bjola C. Digital diplomacy as world disclosure: the case of the COVID-19 pandemic. *Place Brand Public Dipl* 2022;18(1):22 – 5. <https://doi.org/10.1057/s41254-021-00242-2>.
3. Kim HK, Ahn J, Atkinson L, Kahlor LA. Effects of COVID-19 misinformation on information seeking, avoidance, and processing: a

- multicountry comparative study. *Sci Commun* 2020;42(5):586 – 615. <https://doi.org/10.1177/1075547020959670>.
4. World Health Organization. Joint external evaluation tool: international health regulations (2005). 3rd ed. Geneva: World Health Organization. 2022.
  5. WHO E. 2nd Joint External Evaluation of Pakistan. Egypt, Cairo: WHO, EMRO Office; 2024.
  6. Zarocostas J. How to fight an infodemic. *Lancet* 2020;395(10225):676. [https://doi.org/10.1016/S0140-6736\(20\)30461-X](https://doi.org/10.1016/S0140-6736(20)30461-X).
  7. ECDC. HEPSA – health emergency preparedness self-assessment tool, User guide. Stockholm: European Centre for Disease Prevention and Control; 2018 Jun. Report No.: TQ-02-18-883-EN-N.
  8. World Health Organization. WHO benchmarks for strengthening health emergency capacities. Geneva: World Health Organization; 2023 Dec. Report No.: CC BY-NC-SA 3.0 IGO.
  9. Napier NZJNZ. Ministry of Civil Defence and Emergency Management. 2018.
  10. Donelle L, Comer L, Hiebert B, Hall J, Shelley JJ, Smith MJ, et al. Use of digital technologies for public health surveillance during the COVID-19 pandemic: a scoping review. *Digit Health* 2023;9:20552076231173220. <http://dx.doi.org/10.1177/20552076231173220>.
  11. Wong A, Ho S, Olusanya O, Antonini MV, Lyness D. The use of social media and online communications in times of pandemic COVID-19. *J Intensive Care Soc* 2021;22(3):255 – 60. <https://doi.org/10.1177/1751143720966280>.
  12. Văduva LL, Nedelcu AM, Stancu D, Bălan C, Purcărea IM, Gurău M, et al. Digital technologies for public health services after the COVID-19 pandemic: a risk management analysis. *Sustainability* 2023;15(4):3146. <https://doi.org/10.3390/su15043146>.
  13. Purnat T, Bertrand-Ferrandis C, Yau B, Ishizumi A, White B, Briand S, et al. Training health professionals in infodemic management to mitigate the harm caused by infodemics. *Eur J Public Health* 2022;32(Suppl 3):ckac129.324. <https://doi.org/10.1093/eurpub/ckac129.324>.
  14. Ryan B, Johnston KA, Taylor M, McAndrew R. Community engagement for disaster preparedness: a systematic literature review. *Int J Disaster Risk Reduct* 2020;49:101655. <https://doi.org/10.1016/j.ijdrr.2020.101655>.
  15. Tangcharoensathien V, Calleja N, Nguyen T, Purnat T, D'Agostino M, Garcia-Saiso S, et al. Framework for managing the COVID-19 infodemic: methods and results of an online, crowdsourced WHO technical consultation. *J Med Internet Res* 2020;22(6):e19659. <https://doi.org/10.2196/19659>.

## SUPPLEMENTARY MATERIAL

SUPPLEMENTARY TABLE S1. Demographic and departmental information of the respondents.

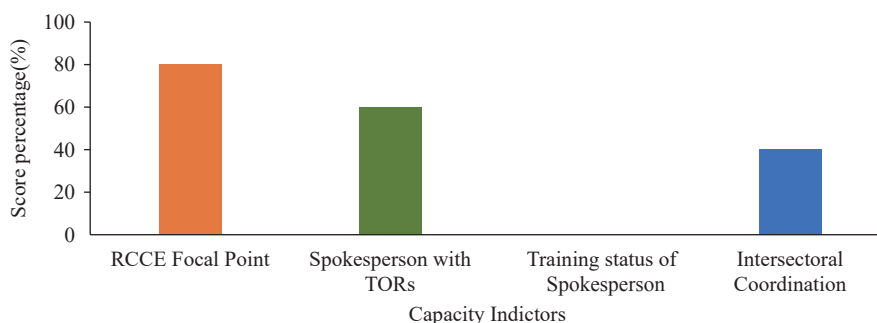
Sr. #	Name	Designation	Organization	Unit/field	Area of operations
1.	Respondent 1	Surveillance coordinator	Department of Health	IDSRS	Disease surveillance and response
2.	Respondent 2	Health education officer	Department of Health, KP	Media information wing	Public information and media
3.	Respondent 3	PRO	Information and media	Media information wing	Public information and media
4.	Respondent 4	DDO training	Department of Health, KP	Public Health Emergencies	FETP and workforce
5.	Respondent 5	Deputy Director, Programs	Department of Health, KP	Coordination and PHEOC management	FETP and Workforce
6.	Respondent 6	Public health officer	Department of Health, KP	PDSRU, PHEOC	Emergency management
7.	Respondent 7	Public health officer	Department of Health, KP	PDSRU, PHEOC	Emergency management
8.	Respondent 8	Public health officer	Department of Health, KP	PDSRU, PHEOC	Emergency management
9.	Respondent 9	Public health officer	Department of Health, KP	PDSRU, PHEOC	Surveillance and response
10.	Respondent 10	Surveillance data coordinator	Department of Health, KP	IDSRS	Disease surveillance and response
11.	Respondent 11	One Health officer	Livestock Department, KP	Livestock Department, KP	One Health coordination
12.	Respondent 12	Veterinary officer	Livestock Department, KP	Livestock Department, KP	Zoonotic disease response
13.	Respondent 13	Provincial staff officer	EPI KP	EPI and vaccination	Immunization and vaccination
14.	Respondent 14	Scientific officer	Climate Change, Forestry, Environment & Wildlife	Climate change and public relation	Public relation
15.	Respondent 15	WHO KP Office	WHO provincial officer	Emergency management	Information management and media
16.	Respondent 16	Program officer capacity building	WHO provincial officer	WHO	Surveillance and response
17.	Respondent 17	Program officer	UNICEF	Public information	Community engagement and risk communication
18.	Respondent 18	Coordinator	USAD-JSI country office	Public health surveillance	Surveillance and response
19.	Respondent 19	Communication coordinator	EMPHNET Office KP	Communication and community engagement	RCCE

Abbreviation: DDO=deputy district officer; PRO=public relations officer; IDSRS=integrated disease surveillance and response system; PDSRU=provincial disease surveillance and response unit; PHEOC=public health emergency operations center; FETP=field epidemiology and training program; EPI=expanded program on immunization.

SUPPLEMENTARY TABLE S2. Scoring guide and achievement scale for capacity and capabilities.

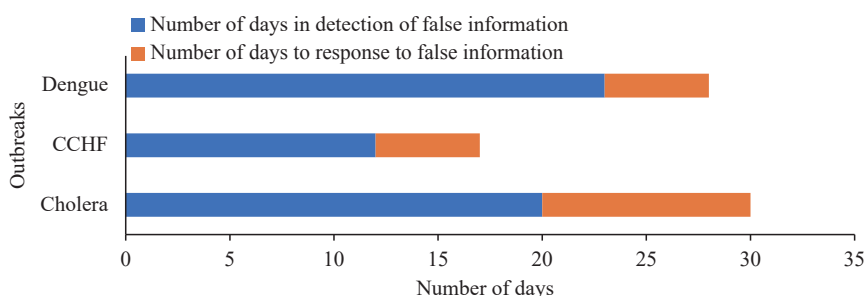
Score	Frequency scale	Achievement scale and attributes
No (0%)	Never	Not started, absence of work or activities
20%	Infrequently	Minimal advancement, initial stages (i.e., started by partners or government without dedicated staff or funding approved)
40%	Sometimes	Some progress but with a lack of a systematic approach (partner funded and absence of domestic funding or staff)
60%	Often	Organizational commitment attained (some level of government staff and funding dedicated) or considerable progress made, but achievements are not yet comprehensive of needs or requirements
80%	Mostly	Substantial achievement with dedicated staff but some recognized limitations in capacities, capabilities and/or resources
Yes (100%)	Always	Comprehensive achievement with sustained commitment and capacities at all levels (capacity or capability fulfill in indicators)

Note: This table presents the scoring guide and achievement scale used to assess the health department's capacities and capabilities. The scoring system employs a frequency-based scale with corresponding analytical values ranging from 0% to 100% (0%, 20%, 40%, 60%, 80%, 100%).



SUPPLEMENTARY FIGURE S1. RCCE Coordination System in Place at Health Department Khyber Pakhtunkhwa

Note: This bar graph depicts the preparedness capacity of the Khyber Pakhtunkhwa Health Department’s infodemic management system across multiple indicators. The y-axis displays the preparedness score in percentage (0–100%), while the x-axis presents the distinct components of the RCCE coordination system.



SUPPLEMENTARY FIGURE S2. Outbreak Response and Infodemic Management from July 2023 to August 2024 by Health Department.

Note: This bar graph compares the outbreak response and infodemic management efforts of the Health Department for three different outbreaks: Dengue, Crimean Congo Hemorrhagic Fever (CCHF), and Cholera focusing on the timeline of the detection and response to false information. The y-axis represents the number of days, while the x-axis shows the different outbreaks.

## Methods and Applications

# A Prediction Model and Method for Indoor Radon Concentration by A Radon Simulation Chamber

Shuyuan Liu<sup>1</sup>; Li Zhang<sup>2</sup>; Wei Cheng<sup>3</sup>; Yongzhong Ma<sup>4</sup>; Kuke Ding<sup>1,2,#</sup>

## ABSTRACT

**Introduction:** This study aimed to establish a new predictive model for indoor radon concentrations.

**Methods:** We constructed a radon experimental model using prefabricated block walls and measured surface radon exhalation rates across multi-layer walls. The geometric parameters of various building envelopes (walls, floors, and roofs) were incorporated to calculate indoor radon concentrations from each source. Natural ventilation rates were also considered in developing the indoor radon concentration prediction model.

**Results:** Using closed-loop measurements, we determined the surface radon exhalation rates of prefabricated block walls and established fitting functions for multiple walls under varying temperatures and thicknesses. Based on indoor geometric parameters and natural ventilation rates, we developed a comprehensive prediction model for indoor radon concentrations. The model accurately predicted indoor equilibrium radon concentrations from prefabricated walls (thickness 0.155–0.268 m) at 23 °C, with deviations less than 10% from measured values within ventilation rates of  $0.115 \pm 0.015$  /h.

**Conclusions:** This scientifically rigorous and practical approach to predicting radon concentration, based on building composition and measurements of radon exhalation rates, enables proactive assessment of indoor radon concentrations and facilitates evidence-based health risk prevention strategies.

Radon ( $^{222}\text{Rn}$ ), a naturally occurring radioactive gas, is the second leading cause of lung cancer and has been associated with leukemia (1–4). The concentration of indoor radon has become an increasing public health concern. To protect public health, it is essential to incorporate predictive modeling of indoor radon levels during the architectural design phase. Such modeling enables optimal selection of

building locations, appropriate sizing of doors and windows, and evidence-based selection of construction materials. By optimizing building structural parameters, it becomes possible to prevent elevated indoor radon levels before construction completion, thereby safeguarding public health. Therefore, developing an accurate indoor radon concentration prediction model is crucial.

## METHODS

### Prefabrication of the Block Walls and Construction of A Radon Experimental Model

A device for measuring radon concentration is illustrated in Figure 1. The prefabricated block wall was sealed by applying an anti-radon coating to four or five surfaces, leaving one or two surfaces exposed for testing.

### Calculation of the Surface Radon Exhalation Rate from Various Source Items in Indoor Buildings

To determine indoor radon concentrations originating from building envelopes, we first established a fitting function for radon exhalation rate as a function of temperature and thickness using multivariate nonlinear regression analysis. We then calculated the total radon contribution by multiplying the surface area of each building envelope by its respective radon exhalation rate. For structures with curved interior surfaces, as illustrated in Figure 2, we employed geometric transformation relations to compute the effective surface area.

### Establishment of a Prediction Model for Indoor Radon Concentration Under Natural Air Exchange Conditions

We developed a prediction model for indoor radon concentration that accounts for radon exhalation rate

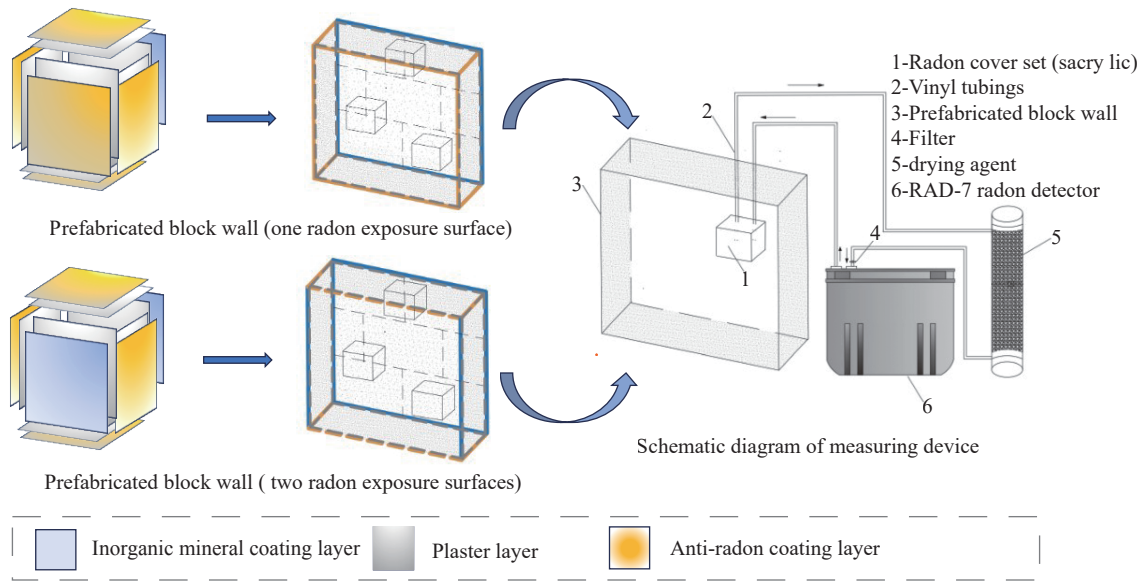


FIGURE 1. Schematic diagram of prefabricated block wall and experimental setup.

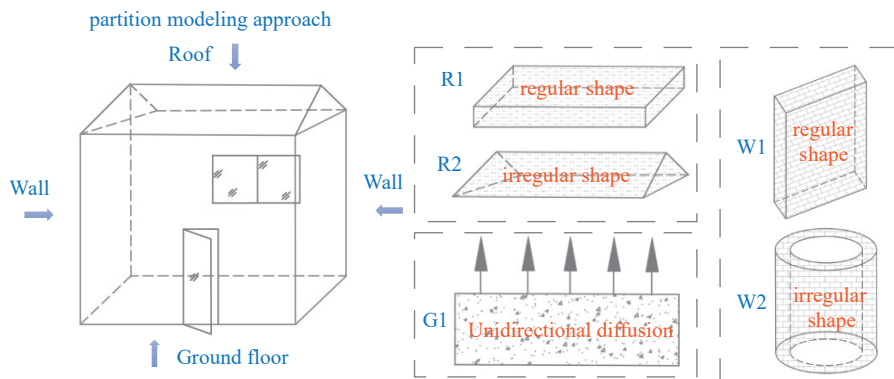


FIGURE 2. A schematic diagram illustrating the overall spatial structure of an indoor environment, including the shapes of different main building envelopes.

Notes: R1 is the roof of regular shape; R2 is the roof of irregular shape; W1 is the wall of regular shape; W2 is the wall of irregular shape; G1 is the ground floor.

from each building envelope at varying temperatures and thicknesses under conditions where building materials are the primary radon source and windows and doors remain closed. For scenarios where the bottom layer consists of soil and outdoor radon primarily originates from soil exhalation, we derived an expression for indoor radon concentration under ventilated conditions with open windows.

## RESULTS

### Measurement of Radon Activity Concentration and Surface Radon Exhalation Rate Fitting Function

Using autoclaved concrete blocks as raw materials,

we measured the surface radon exhalation rates of prefabricated block walls (one radon exposure surface) at three distinct thicknesses and five constant temperatures. Based on these measurements, we developed a fitting function to characterize the relationship between radon exhalation rate and the variables of temperature and wall thickness. The resulting fitting model is illustrated in Figure 3, with the corresponding mathematical expression presented in Equation (1).

$$H(X_{si}, T_{sj}) = -78.49982 + 804.1884X_{si} - 0.091T_{sj} - 1703.19947X_{si}^2 + 1.05192X_{si} \cdot T_{sj} \quad (1)$$

$T_{sj}(R^2 = 0.93376)$

In Equation (1),  $H(X_{si}, T_{sj})$  represents the surface radon exhalation rate of the building envelope within

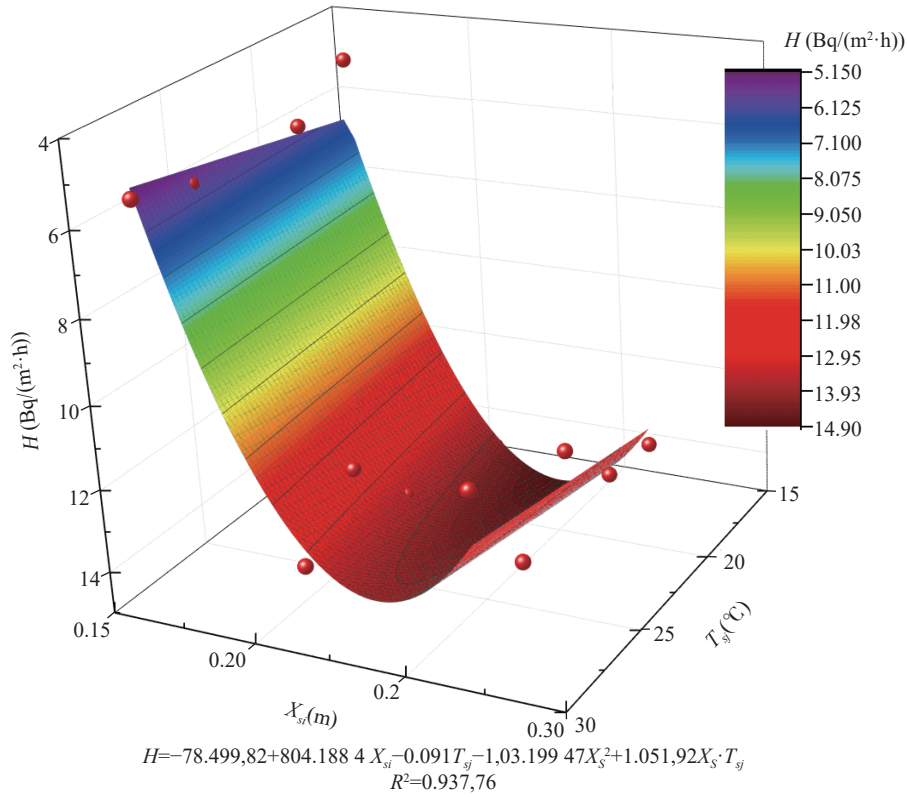


FIGURE 3. The fitting model of surface radon exhalation rate of block walls with varying temperatures and thicknesses. Notes:  $H$  is the radon exhalation;  $X_{si}$  is the structural thickness;  $T_{sj}$  is the indoor temperature;  $R^2$  is the goodness of fit.

the target room ( $\text{Bq}/(\text{m}^2 \cdot \text{h})$ );  $X_{si}$  denotes the thickness of the building envelope (m); and  $T_{sj}$  indicates the indoor temperature ( $^{\circ}\text{C}$ ).

### Expression for the Surface Radon Exhalation Rate from Walls with Multiple Materials

The total radon exhalation rate in walls composed of multiple materials can be expressed as the superposition of individual radon exhalation rates from each constituent material.

$$H(X_{si}, T_{sj}) = \frac{\sum_{k=1}^{k=z} H(X_{si}, T_{sj}) S_{sk}}{S} \quad (2)$$

In Equation (2),  $S_{sk}$  represents the actual exposed surface area ( $\text{m}^2$ ) of a specific material within the building envelopes;  $z$  represents kinds of materials;  $S$  denotes the total surface area of all building envelopes.

Surface area calculations vary by the type of building envelopes. For regular rectangular walls, as follows:

$$S_{sk1} = \theta_b \times \theta_w \quad (3)$$

Where,  $S_{sk1}$  is the actual exposed surface area of regular rectangular wall ( $\text{m}^2$ );  $\theta_b$  represents the height of wall (m);  $\theta_w$  represents the width of wall (m).

For building envelopes with curved interior surfaces, surface area calculations utilize geometric transformation relations, such as irregular arc walls, the structure is transformed into a cylindrical cavity, as follows:

$$S_{sk2} = \varepsilon_c h_c \quad (4)$$

Where,  $\varepsilon_c = 2\pi r_c$ ,  $S_{sk2}$  is the actual exposed surface area of irregular arc wall ( $\text{m}^2$ );  $\varepsilon_c$  represents the length of each curve (m);  $h_c$  represents the height of wall (m).

### Expression of A Prediction Model for Indoor Radon Concentration

For rooms where indoor radon primarily originates from construction materials, the radon concentration under natural air exchange conditions can be expressed by the following equation:

$$C(t) = \frac{H(X_{si}, T_{sj})S + \eta V_{eff} C_0}{\lambda_{eff} V_{eff}} + \left( \frac{H(X_{si}, T_{sj})S + \eta V_{eff} C_0}{\lambda_{eff} V_{eff}} - C_0 \right) e^{-(\lambda + R + \eta)t} \quad (5)$$

In Equation (5),  $C(t)$  represents the radon concentration ( $\text{Bq}/\text{m}^3$ );  $\lambda_{eff}$  is the effective decay constant (1/s);  $\lambda_{eff} = \lambda_{Rn} + R + \eta$ , 1/s;  $\lambda_{Rn}$  denotes the

radon decay constant,  $\lambda_{Rn} = 0.00756/h$ ;  $R$  represents the inverse diffusion coefficient, which characterizes the diffusion of indoor air radon into construction materials (1/s);  $\eta$  is the ventilation rate (1/h); and  $V_{eff}$  represents the effective room volume, defined as the total room volume minus the volume occupied by objects ( $m^3$ );  $C_0$  is the background radon concentration ( $Bq/m^3$ ).

When sufficient time has elapsed for indoor radon accumulation to reach equilibrium, the concentration can be calculated using:

$$C_{equ} = \frac{H(X_{si}, T_{sj})S + \eta V_{eff} C_0}{\lambda_{eff} V_{eff}} \quad (6)$$

In Equation (6),  $C_{equ}$  represents the concentration when indoor radon accumulation to reach equilibrium ( $Bq/m^3$ ). In typical residential buildings, the indoor ventilation rate exceeds the radon decay rate by more than two orders of magnitude. Therefore, both the radon decay and indoor anti-diffusion effects can be neglected, yielding  $\lambda_{eff} = \lambda_{Rn} + R + \eta \approx \eta$ . Under these conditions, Equation (6) simplifies to:

$$C_{equ} = \frac{H(X_{si}, T_{sj})S}{\eta V_{eff}} + C_0 = C_{H(X_{si}, T_{sj})} + C_0 \quad (7)$$

In Equation (7),  $C_{H(X_{si}, T_{sj})}$  is defined as the indoor radon concentration contributed by construction materials, which can be calculated using:

$$C_{H(X_{si}, T_{sj})} = \frac{H(X_{si}, T_{sj})S}{\eta V_{eff}} = \frac{\sum_{k=1}^{k=z} H(X_{si}, T_{sj})S_{sk}}{\eta V_{eff}} \quad (8)$$

The comprehensive expression for indoor radon concentration is:

$$C = \frac{\sum_{k=1}^{k=z} H(X_{si}, T_{sj})S_{sk}}{\eta V_{eff}} + C_0 \quad (9)$$

In Equation (9),  $C$  is defined as the indoor radon concentration ( $Bq/m^3$ ). For scenarios where the bottom layer consists of soil, the indoor radon concentration can be expressed as:

$$\phi(t) = \frac{\sum_{k=1}^{k=z} H(X_{si}, T_{sj})S_{sk} + \eta V_{eff} C_d}{\lambda_{eff} \lambda_{eff}} + \left( C_0 - \frac{\sum_{k=1}^{k=z} H(X_{si}, T_{sj})S_{sk} + \eta V_{eff} C_d}{\lambda_{eff} \lambda_{eff}} \right) e^{-\lambda_{eff} t} \quad (10)$$

In Equation (10),  $\phi(t)$  represents the total indoor radon concentration with a soil bottom layer in  $t$  time ( $Bq/m^3$ ), while  $C_d$  denotes the outdoor radon concentration generated by the soil layer ( $Bq/m^3$ );  $t$  represents time (h).

Given that  $\lambda_{eff} = \lambda_{Rn} + R + \eta \approx \eta$  and  $e^{-(\lambda+R+\eta)t} \approx 0$ , Equation (10) can be simplified to:

$$\phi = \frac{\sum_{k=1}^{k=z} H(X_{si}, T_{sj})S_{sk}}{\eta V_{eff}} + C_d \quad (11)$$

In Equation (11),  $\phi$  represents the total indoor radon concentration with a soil bottom layer ( $Bq/m^3$ ).

## The Application of the Prediction Model for Indoor Radon Concentration

We applied the prediction model for indoor radon concentration from construction materials to a radon simulation chamber (container house). Five prefabricated block walls of varying thicknesses (0.155 m, 0.165 m, 0.172 m, 0.213 m, and 0.268 m) as the sole radon sources within the chamber. The interior dimensions of the chamber measured  $2.80 \times 5.80 \times 2.50 m^3$ , featuring one door ( $0.90 \times 1.9 m^2$ ) and two windows ( $0.86 \times 0.93 m^2$ ). The effective volume of the chamber was  $38.78 m^3$ , representing 96% of the total interior volume. Temperature control was maintained using an air conditioning system.

During the winter experiment, doors and windows remained closed, resulting in low ventilation rates (5–7), which were approximated at 0.10–0.12 /h.

We calculated the indoor radon concentration under different ventilation rates at 23 °C and compared these values with the measured equilibrium radon concentration at the same temperature. The background radon concentration was  $6.50 Bq/m^3$ . The results are presented in Table 2.

## DISCUSSION

Indoor radon primarily originates from soil and building materials (8). Two critical factors influence indoor radon accumulation: surface radon exhalation rate and ventilation rate (9–11). We have established a prediction model for indoor radon concentration that incorporates the internal surface area and radon exhalation rate of the building envelope, indoor temperature, and natural air exchange rate, enabling accurate calculation of indoor radon concentration

TABLE 1. Comparison of calculated and measured radon concentration when equilibrium.

Ventilation rate (1/h)	Theoretical value (Bq/m <sup>3</sup> )	Measured value (Bq/m <sup>3</sup> )	Deviation (%)
0.10	21.25		7.76
0.11	19.91	19.60	1.56
0.12	18.80		4.26
0.13	17.85		9.80

under the combined influence of multiple factors.

A key strength of this model lies in its integration of building structural geometric parameters and environmental factors affecting indoor radon concentration. We developed a correlational function that accounts for radon exhalation rates across multiple walls at varying temperatures and thicknesses. The relationship between construction materials and indoor radon concentration has been optimized through direct measurement of surface radon exhalation rates from prefabricated walls, significantly enhancing the accuracy and broader applicability of indoor radon concentration predictions. For building envelopes with curved interior surfaces, we employed geometric transformation relationships to calculate wall surface areas. Through comparative analysis and validation, we demonstrated that the model's estimated indoor radon concentration from walls with thicknesses of 0.155–0.268 m at 23 °C aligns with measured values, with deviations less than 10%.

This refined model provides valuable guidance for preliminary building site selection, optimal door and window dimensioning, and scientifically informed selection of construction materials with respect to radon safety considerations.

While the model has limitations regarding daily and seasonal wall temperature fluctuations, as the fitting curve for exhalation rate calculations was derived from constant-temperature experiments, these constraints can be addressed by incorporating multiple fitting curves for various temperatures and wall thicknesses. Although there exists a discrepancy between modeled and real-world conditions, this deviation remains theoretically insignificant. Thus, the model maintains its practical utility and scientific validity within a controllable range.

**Conflicts of interest:** No conflicts of interest.

**Ethical Statements:** This research involves no ethical concerns as it does not include human/animal subjects or sensitive data.

doi: 10.46234/ccdcw2025.061

# Corresponding author: Kuke Ding, dingkk@chinacdc.cn.

<sup>1</sup> National Institute for Radiological Protection, Chinese Center for Disease Control and Prevention, Beijing, China; <sup>2</sup> Office for Public

Health Management, Chinese Center for Disease Control and Prevention, Beijing, China; <sup>3</sup> Key Laboratory of Beam Technology of Ministry of Education, School of Physics and Astronomy, Beijing Normal University, Beijing, China; <sup>4</sup> Institute for Radiation Hygiene Protection, Beijing Center for Disease Prevention and Control, Beijing, China.

Copyright © 2025 by Chinese Center for Disease Control and Prevention. All content is distributed under a Creative Commons Attribution Non Commercial License 4.0 (CC BY-NC).

Submitted: February 23, 2024

Accepted: February 24, 2025

Issued: March 14, 2025

## REFERENCES

1. Ting DSK. WHO handbook on indoor radon: a public health perspective. *Int J Environ Stud* 2010;67(1):100 – 2. <https://doi.org/10.1080/00207230903556771>.
2. Abbasi A, Mirekhtiary F, El-Denglawey A, Zakaly HMH. Influences of COVID-19 pandemic lockdown on excess lifetime cancer risk value of natural radiation. *J Radioanal Nucl Chem* 2021;329(3):1399 – 406. <https://doi.org/10.1007/s10967-021-07910-w>.
3. Ruano-Ravina A, Lema LV, Talavera MG, Gómez MG, Muñoz SG, Santiago-Pérez MI, et al. Lung cancer mortality attributable to residential radon exposure in Spain and its regions. *Environ Res* 2021;199:111372. <https://doi.org/10.1016/j.envres.2021.111372>.
4. Gooding TD. An analysis of radon levels in the basements of UK workplaces and review of when employers should test. *J Radiol Prot* 2018;38(1):247 – 61. <https://doi.org/10.1088/1361-6498/aaa18c>.
5. Chen YH, Chen YL, Wang QX, Li ZX, Chen P. Investigation and research on ventilation of naturally ventilated residences in China. *Heat Vent Air Cond* 2020;50(12):85 – 8,19. <https://doi.org/10.19991/j.hvac.1971.2020.12.021>.
6. Hong YF, Dai ZZ, Chen X, Shen SL. Estimation of air exchange frequency in the condition of natural indoor ventilation. *J Environ Health* 2005;22(1):47 – 9. <https://doi.org/10.3969/j.issn.1001-5914.2005.01.018>.
7. Tan YL. Research on threshold value of average radon exhalation rate from indoor surface. *J Hengyang Norm Univ* 2016;37(3):30 – 3. <https://doi.org/10.13914/j.cnki.cn43-1453/z.2016.03.008>.
8. Mancini S, Guida M, Cuomo A, Guida D, Ismail AH. Modelling of indoor radon activity concentration dynamics and its validation through in-situ measurements on regional scale. *AIP Conf Proc* 2018;1982(1):020043. <https://doi.org/10.1063/1.5045449>.
9. Yarmoshenko I, Malinovsky G, Vasilyev A, Onishchenko A. Model of radon entry and accumulation in multi-flat energy-efficient buildings. *J Environ Chem Eng* 2021;9(4):105444. <https://doi.org/10.1016/j.jece.2021.105444>.
10. Sahoo BK, Nathwani D, Eappen KP, Ramachandran TV, Gaware JJ, Mayya YS. Estimation of radon emanation factor in Indian building materials. *Radiat Meas* 2007;42(8):1422 – 5. <https://doi.org/10.1016/j.radmeas.2007.04.002>.
11. Shahrokhi A, Kovacs T. Radiological survey on radon entry path in an underground mine and implementation of an optimized mitigation system. *Environ Sci Eur* 2021;33(1):66. <https://doi.org/10.1186/s12302-021-00507-w>.

## Youth Editorial Board

**Director** Lei Zhou

**Vice Directors** Jue Liu    Tiantian Li    Tianmu Chen

### Members of Youth Editorial Board

Jingwen Ai	Li Bai	Yuhai Bi	Yunlong Cao
Gong Cheng	Liangliang Cui	Meng Gao	Jie Gong
Yuehua Hu	Jia Huang	Xiang Huo	Xiaolin Jiang
Yu Ju	Min Kang	Huihui Kong	Lingcai Kong
Shengjie Lai	Fangfang Li	Jingxin Li	Huigang Liang
Di Liu	Jun Liu	Li Liu	Yang Liu
Chao Ma	Yang Pan	Zhixing Peng	Menbao Qian
Tian Qin	Shuhui Song	Kun Su	Song Tang
Bin Wang	Jingyuan Wang	Linghang Wang	Qihui Wang
Xiaoli Wang	Xin Wang	Feixue Wei	Yongyue Wei
Zhiqiang Wu	Meng Xiao	Tian Xiao	Wuxiang Xie
Lei Xu	Lin Yang	Canqing Yu	Lin Zeng
Yi Zhang	Yang Zhao	Hong Zhou	

Indexed by Science Citation Index Expanded (SCIE), Social Sciences Citation Index (SSCI), PubMed Central (PMC), Scopus, Chinese Scientific and Technical Papers and Citations, and Chinese Science Citation Database (CSCD)

**Copyright © 2025 by Chinese Center for Disease Control and Prevention**

Under the terms of the Creative Commons Attribution-Non Commercial License 4.0 (CC BY-NC), it is permissible to download, share, remix, transform, and build upon the work provided it is properly cited. The work cannot be used commercially without permission from the journal.

References to non-China-CDC sites on the Internet are provided as a service to *CCDC Weekly* readers and do not constitute or imply endorsement of these organizations or their programs by China CDC or National Health Commission of the People's Republic of China. China CDC is not responsible for the content of non-China-CDC sites.

The inauguration of *China CDC Weekly* is in part supported by Project for Enhancing International Impact of China STM Journals Category D (PIIJ2-D-04-(2018)) of China Association for Science and Technology (CAST).



*Vol. 7 No. 11 Mar. 14, 2025*

---

**Responsible Authority**

National Disease Control and Prevention Administration

**Sponsor**

Chinese Center for Disease Control and Prevention

**Editing and Publishing**

China CDC Weekly Editorial Office  
No.155 Changbai Road, Changping District, Beijing, China  
Tel: 86-10-63150501, 63150701  
Email: weekly@chinacdc.cn

**CSSN**

ISSN 2096-7071 (Print)

ISSN 2096-3101 (Online)

CN 10-1629/R1